Scientific Reports

https://doi.org/10.1038/s41598-026-40420-x

Article in Press

Short-term modulation of mineral phosphorus fractions by functionalized biochars in different alkaline soil types

Received: 16 August 2025

Accepted: 12 February 2026

Published online: 18 March 2026

Cite this article as: Fathy R., Elagroudi W., Taha A.A. *et al.* Short-term modulation of mineral phosphorus fractions by functionalized biochars in different alkaline soil types. *Sci Rep* (2026). https://doi.org/10.1038/s41598-026-40420-x

Radwa Fathy, Wagdi Elagroudi, Ahmed A. Taha & Ahmed Mosa

Short-term modulation of mineral phosphorus fractions by functionalized biochars in different alkaline soil types

Radwa Fathy[a], Wagdi Elagroudi[a], Ahmed A. Taha[a], Ahmed Mosa[a,*]

[a] Soils Department, Faculty of Agriculture, Mansoura University, Mansoura 35516, Egypt

*Corresponding author:

E-mail address: ahmedmosa@mans.edu.eg

Cell phone:+201004441278

Abstract

There remains a gap of knowledge regarding the functionalization of modified biochar types to enhance phosphorus (P) availability in arid soils. Therefore, original biochar (OB) derived from pyrolyzed *Dodonaea viscosa* feedstock at 500 ^{o}C was functionalized using ball milling (BMB), chemical oxidation (CHB), and biological activation (BIOB) to study their short-term effect on mineral P dynamics in charosphere of different soil types. Elemental and XRD analyses of OB and BIOB pointed to considerable amounts of P (0.95 and 0.71%) with a presence of P-containing minerals. EDS spectra of BIOB-amended soils showed elevated peaks of C (61.39–76.94%) confirming the exterior coating of soil granules by modified biochar through biofilm formations of extracellular polymeric substances secreted by the niche of B. *subtilis*. Biochar application motivated the formation of microaggregate fractions (the main sink of orthophosphates; <0.25–0.05 mm) relative to unamended treatment. Fractional amounts of different P forms showed alterations following biochar application with a significant increase of the labile P pool, including soluble (53.86–870.25%) and exchangeable (92.71–982.92%) fractions. The high functionality of modified biochars modulated P dynamics in the soil-biota-plant system through secretion of solubilizing compounds (BIOB), increasing soil wettability and controlling the strength of reactive metal ions responsible for phosphate fixation (BMB), and releasing of acidifying compounds responsible for amending soil pH (CHB). Modulating effects of biochar on P dynamics in the soil-biota-plant system was able to transform higher amounts of residual P fractions

into labile forms relative to the soil-biota system. Biochar application enhanced soil's potential to supply phytoavailable nutrients to maize seedlings. Findings from this study, therefore, provide insights regarding functionalization of fit–for–purpose forms of modified biochar tailored in improving P phytoavailability in arid soils.

Keywords: Functionalized biochar; Modulation; Orthophosphates; Rhizosphere; Phytoavailability

1. Introduction

Phosphorus is a functional indispensable macronutrient for the optimal nutrition of living organisms. It has a paramount importance in multiple physiological processes including cell division, energy dynamics (trapping, transportation and donation), photosynthesis, phosphorylation, plasma membrane synthesis, root development and plant resilience to abiotic/abiotic stresses [1]. The average value of the global total P concentration in soil is estimated as 570 mg kg^{-1} [2]. However, only 10–25% of the applied P fertilizers are taken up by plants in forms of orthophosphates ($H_2PO_4^-$, HPO_4^{2-} and H_3PO_4) due to its high fixation by several soil components including calcium carbonate ($CaCO_3$), iron (Fe) and aluminum (Al) (oxyhydr)oxides, and soil organic matter [3]. In this regard, calcium carbonate is proven as the most contributing component for minimizing P phytoavailability in arid and semi-arid regions [4]. This low use efficiency resorted agricultural workers to extravagance in mineral P fertilizers application to cope with plant requirement. This overuse application of mineral P fertilizers led to

significant financial burdens and environmental deteriorations in the ecosphere (e.g. changing diversity of the biosphere, increasing salinity of the rhizosphere and eutrophication of the hydrosphere) [5]. Consequently, the conversion of the hidden treasure of insoluble phosphates into available orthophosphate forms became an exciting research problem worldwide.

Several agricultural strategies have been adopted for exploitation of residual P reservoirs (legacy P), including organic amendments application [6], microbial inoculation [7], breeding P-efficient plant varieties [8], evolving modern farming systems [9] and utilization of microemulsions [10]. Of these, organic amendments (animal wastes, crop residuals, green manures, sewage sludge, household wastes and industrial wastes) have paid intensive research attention given their renewability, long-lasting, and simple–to–design potentials. However, a great deal of uncertainty arises surrounding the high greenhouse gases footprint of these amendments [11], their high pollution potential [12], and their high load of pathogens and weed seeds [13]. In addition, organic amendments application might cause P-induced eutrophication due to the co-migration of phosphates with dissolved organic carbons/metal ions and enhancing the migration of organic/inorganic P into leachates [14].

Recently, biochar (a charcoal-like material originated from the thermochemical conversion of organic biomass under limited or no oxygen conditions) has become the focal point of several agro-environmental applications [15]. The unique functionality of biochar (e.g. its porous structure, high surface area, and abundance of active functional groups) provides a

convenient medium for growth of P-solubilizing microorganisms [16]. Worth noting, biochar has the ability to modulate physicochemical and biological properties (e.g., aeration, water holding capacity, aggregation, pH, nutrient supply potentials, microbial activity/biodiversity, and labile carbon (C) pool) of alkaline/calcareous soils. This indirectly promote activity of several bacterial genera involved in mineral phosphate solubilization and organic P mineralization [17]. Besides, the competition between P and humic substances derived from biochar might promote the exchangeability and availability of P in soil [18]. Biochar application to alkaline/calcareous soils can also minimize the affinity between orthophosphates and active soil constitutions responsible for their precipitation (calcium carbonate in particular). Additionally, the abundance of active functional groups onto biochar surfaces might interact with soluble calcium ions (Ca^{2+}) responsible for phytoavailable P fixation [19]. Consequently, there is an urgent need to understand modulating effects of biochar on soil P dynamics in soil-biota and soil-biota-plant system, particularly in alkaline and calcareous soils.

The functionality of biochar greatly depends upon its feedstock source. Previous studies highlight high P sorptivity of biochars derived from different sources including rice straw [20], bamboo [21], and almond and walnut shells [22]. However, the strong chemisorption forces responsible for P binding onto the carbonaceous lattice of biochar might reduce phosphate desorbability/exchangeability. Therefore, it is urgently needed to produce biochars with less binding force and high desorbability potential to avoid the

short-term retardation of P phytoavailability in the charosphere. *Dodonaea viscosa* feedstock contains various bioactive compounds (e.g. alkaloids, flavonoids, tannins, triterpenoids, steroids, saponins, phytosterols and volatile oils), which boost its potential utilization as an adsorbent material [23]. Additionally, Yaqub et al's study highlighted the high desorbability and recyclability potential of activated carbon derived from *Dodonaea Viscosa* [24]. Consequently, residuals of this plant might act as a promising feedstock material for tailoring functionalized biochars to modulate P dynamics and maximize phytoavailability of orthophosphates.

Despite the efficacy of some feedstock materials in biochar engineering, several functionalization techniques have been introduced during the last decade to produce highly efficient biochars tailored in maximizing phosphate phytoavailability in different soil types. Ball milling is considered as a non-sophisticated physical modification method for improving the functionality of biochar, including its surface area, porosity, graphitic structure, hydrophilicity and polarity [25]. Furthermore, ball milled biochar can limit P fixation in soil through controlling the strength of reactive metal ions such as Ca^{2+}, Fe^{3+} and Al^{3+} [26]. In addition, the development of manganese oxide-modified biochars might maximize the bioavailability/reusability of P-loaded biochar through reducing the high binding of sorbed P ions onto the carbonaceous lattice of biochar to improve its desorbability potential [27]. Biochar was also exploited for recovery and reuse of phosphate from aqueous solutions. For instance, biochar-seeded struvite precipitation technique was

introduced for phosphate recovery from aqueous solution and reutilization as a slow-released P fertilizer [28]. What's more, bacterial loading onto biochar has been recently presented as an innovative technique to improve the performance of biochar toward phosphate solubilization [29]. Due to its unique functionality, biochar matrix could be considered as an optimum shelter for microbial colonization, thanks to its high porosity, low aromaticity, non-biodegradable carbon content, and affordable active functional groups necessarily for microbial cell adhesion and proliferation [30]. Biochar-based slow-release P fertilizers (prepared from microwave pyrolyzed cotton straw), as a case in point, showed a high biocompatibility for loading of phosphate-solubilizing microorganisms (*Enterobacter hormaechei* Rs-198) due to its low aromaticity, graphitization and free radicals' content [31]. This successful loading regulated the release of P from phosphate-enriched biochar through the biofilm formation by Rs-198 that could entrap the release of P in soil in the form of polyphosphate.

Despite the intensive research undertaken for harnessing the full capacity of biochar to improve the phytoavailability of phosphates, there is still a void in knowledge regarding modulating effects of biochar on the fractional amounts of different P forms before and after plantation in different soil types. The novelty aspects of this investigation arise surrounding studying the modulating effects of biochar on P dynamics in soil-biota-plant system as compared with soil-biota system. This might help in providing sufficient knowledge necessarily to synthesis fit–for–purpose forms of functionalized

biochars tailored in improving P phytoavailability in the charosphere. To contextualize the research background of this study, the main overriding objectives are to: (i) engineering and characterization of functionalized biochars with high P content and low P sorptivity, (ii) studying the combination between functionalized biochar and soil particles after its short-term application, (iii) assessing the short-term modulating effects of functionalized biochar on soil P fractions under laboratory microcosm and bioassay experiments, and (iv) assessing the effect of biochar application on plant performance under different soil types.

2. Materials and methods

2.1. Materials

Dodonaea (*Dodonaea Viscosa*) was served as a feedstock material for biochar engineering due to the abundance of bioactive compounds (e.g., alkaloids, flavonoids, tannins, triterpenoids, steroids, saponins, phytosterols and volatile oils). These compounds might stimulate the sorptivity potential of Dodonaea-based biochar [23]. Deionized water (Nanopure water, Barnstead) with a resistivity of 18.2 MΩ was used for preparing chemical solution and rinsing of maize samples. All chemical reagents of analytical grade (Fisher Scientific) were used without further purification. Composite surface samples (0-30 cm depth) were collected from three soil types with different contents of $CaCO_3$: (i) Agricultural Research Farm of Mansoura University, Dakahlia

Governorate (31°02'N 31°21'E; soil a), (ii) Abu Qirqas, Minya Governorate (27º 52'N 30º33'E; soil b) and (iii) Manshiyat Al Qanatir, Giza Governorate (30°10'N, 31°6'E; soil c). Soil samples were collected according to ISO 11464 standard, air-dried, crushed, sieved through a 2–mm sieve and stored for different analysis.

2.2. Biochar preparation

The raw feedstock of biochar (*Dodonaea Viscosa*) was rinsed with deionized water, chopped into a uniform size (~ 0.5–1 mm) and dried using a hot-air oven (70 ±5.0 °C) until reaching mass constancy. The feedstock material was pyrolyzed at 500 ±5.0 °C (5-10 °C min^{-1}), ground manually using a ceramic mortar and sieved to obtain the uniform < 0.5 mm-sized fraction. Original biochar was ball milled to reduce the affinity between orthophosphates and active soil constitutions responsible for their precipitation (calcium carbonate in particular). Ball-milled biochar was prepared with the aid of ball-milling machine equipment supported with 18 balls of porcelain (McCrone Micronizing Mill) at the speed of 50HZ/min for 30 min. Ball milled biochar was sieved using 0.1mm sieve to remove any large particles and labeled as BMB [32]. Chemically modified biochar (CHB) was prepared by chemical oxidation with potassium permanganate ($KMnO_4$) to generate acidifying compounds capable of maintaining phosphate solubilization. CHB was prepared according to El-Banna et al. [33]. Original biochar (250 g) was shaken with $KMnO_4$ (0.1M) at 200 rpm for 4 h at the rate of 1:16 (w:v). Chemically activated biochar was filtered using Whatman filter paper grade 42, washed

with tap water and DI water to remove the excess of $KMnO_4$, air-dried and oven-dried at 70 ±5.0 °C until reaching mass constancy and referenced as CHB.

Biologically activated biochar (BIOB) was prepared to produce bacterial-inoculated form with high capability for secretion of solubilizing compounds. BIOB was functionalized using the protocol of Feng et al. with some modifications [34]. Nutrient agar medium (1.0 g yeasts, 5.0 g peptone, 3.0 g meat extract and 15.0 g agar into 1.0 L ultrapure deionized water at pH value of 7.0 ±0.2) was prepared, sterilized in autoclave for 30 min at 121°C, cooled up to 45 °C, and poured into the sterilized petri dishes. Bacillus colony was grown in the nutrient agar medium and incubated upside down at 22 ^{o}C for 24 h. Thereafter, the pure colony of *Bacillus subtilis* (MFy97446) was grown in nutrient broth media containing 1.0 g L^{-1} yeast, 5.0 g L^{-1} peptone and 3 g L^{-1} meat extract and shaken in a rotary shaker for 48 h at 28 ^{o}C. The inoculation density of bacillus strain was 5×10^{4} CFU/ml. Biochar (250 g) was sterilized in autoclave at 121 ^{o}C for 30 min, soaked in the cell suspension (4 L) at the ratio of 1:16 (w:v) and incubated in rotary shaker for 24 h at 30 ^{o}C. The suspension was filtered using Whatman 42 and the filtrated biochar was collected, oven-dried at 40 ^{o}C for 24 h and referenced as BIOB.

Preliminary experiment was performed in triplicates with different types of biochar (*Dodonaea Viscosa*- hickory chips, raw bagasse and peanut hull) pyrolyzed at different temperatures (300–600 ^{o}C) to select a fit–for–purpose biochar with low sorptivity and high desorbability potentials. Phosphate

sorptivity onto pristine and functionalized biochars was examined using batch sorption experiments with an initial concentration of 50 mg L^{-1} P (KH_2PO_4 salt) in 68mL polypropylene digestion vessels (Environmental Express) at an agitation time of 4 h @ 250 rpm. Sorptivity of functionalized biochars was compared with reported data in Table S1. Furthermore, labile P forms including soluble (H_2O–P) and exchangeable ($NaHCO_3$–P) of pristine and functionalized biochars were also determined. Phosphorus was measured spectrophotometrically at wavelength of 720 nm using a T80 UV–Vis, PG Instruments.

2.3. Biochar characterization

Scanning electron microscope (SEM) visualization was performed using a JEOL JSM 6510 lv. In addition, the surface elemental distribution onto biochars was carried out simultaneously with SEM visualization by an energy dispersive X**-**ray spectroscopy (Oxford X-Max 20) [35]. Total surface area was measured following N_2 sorption Brunauer–Emmett–Teller (BET) method [36]. Besides, pore radius and pore volume values were determined using Barrett–Joyner–Halenda (BJH) pores size distribution analysis. Sorption–desorption isotherms of N_2 were recorded at 77.35 K after outgassing at 200 ^{o}C for 3 h by a Nova-Touch LX4, Quantachrome, USA. Surface functional groups were characterized using Fourier transform infrared spectroscopy (FTIR) [37]. Oven-dried biochar samples (70 ^{o}C for 24 h) were mixed with potassium bromide *(*spectroscopic grade) at the rate of 100:1 (w/w) and the spectra were collected using a Thermo Scientific-Nicolet iS10 at the wave number

ranging between 400–4000 cm^{-1}. FTIR spectra of dissolved humic substances derived from original and pristine biochars were further determined using the same protocol.

X–ray diffraction (XRD) analysis was carried out to identify the crystalline minerals formation onto biochars by computer-controlled X–ray diffractometer (D8 Advance Type, Bruker–AXS) equipped with a stepping motor and graphite crystal monochromator [38]. Thermogravimetric analysis (TGA) was carried out under a stream of air/nitrogen atmosphere between temperatures of 25 and 700 ^{o}C (temperature rate of 10 $^{o}C\ min^{-1}$) with a gas flow of 20 mL min^{-1} using TG/dTG simultaneous measuring instrument (Shimadzu corporation). Differential Scanning Calorimetry (DSC) was determined using SETRAM DSC evo-131 instrument with heating range of 25–600 ^{o}C with a rising temperature rate of 10 ^{o}C/min [39]. Zeta potential (ζ) values of biochars were measured using Zeta potential analyzer (Malvern Zeta size Nano-zs90) in the sonicated distilled water suspension.

Total organic elements including carbon (C), nitrogen (N) sulfur (S) and oxygen (O) were determined using dry combustion technique by a CHNS elemental analyzer (Thermo scientific Flash 2000) [40]. Total inorganic elements were determined by Inductivity Coupled Plasma (iCAPTM 7000 Plus Series ICP–OES, Thermo ScientificTM) after digestion with the acid mixture of nitric acid (HNO_3, 70%) and hydrochloric acid (HCl, 35%) by a microwave digestion apparatus (Milestone MLS 1200 Mega) [41]. Phosphorus concentration in biochar was colorimetrically determined in the digested

solution using a T80 UV–Vis Spectrophotometer at wavelength of 720 nm. Values of biochar's pH were measured using Jenway 3505 pH/mV/Temperature Meter in the biochar suspension (1:20 w/v). The electrical conductivity (EC) values were measured in the extraction of biochar (1:20 w/v) by EC meter (HANNA HI9835).

Point of zero charge (the point where the negative and positive charges are equal) was determined as described by Bakatula, et al. [42]. In brief, 0.05 g of biochar samples was added to 50 ml of 0.1M of potassium nitrate (KNO_3) solution after adjusting the solution's pH at 2.0, 3.0, 4.0, 5.0, 6.0, 7.0, 8.0, 9.0, 10.0 and 11.0 (denoted as pH_i)) by adding 0.1 M of either HNO_3 or potassium hydroxide (KOH) solutions. Biochar suspensions were shaken using rotary shaker for 24h at 200 rpm, filtered and the pH values were measured again and denoted as pH_f. The point of zero charge was obtained from the plot between (Δ pH= pH_f - pH_i) verses pH_i.

2.4. Soil analysis

Soil physical and chemical analyses were carried out according to standard methods. The pipette method was followed for determination of particle size distribution [43]. The gasometric method was used for $CaCO_3$ determination by addition of HCL solution (6.0 M) and utilization of pure $CaCO_3$ (analytical grade) as a reference material [44]. Particle density, bulk density and soil porosity were determined using calculation of mass per unit of given volume [45]. pH meter (Jenway 3505 pH/mV/Temperature Meter) and EC meter (HANNA HI9835) were used for determination of soil reaction and salinity in

soil/water suspension and soil/water extract (1:2.5 w:v), respectively. Soil/water extract was further used for determination of water–soluble cations: sodium (Na^+), potassium (K^+), calcium (Ca^{2+}) and magnesium (Mg^{2+}) and anions: carbonate (CO_3^{2-}), bicarbonate (HCO_3^-), chloride (Cl^-) and Sulphate (SO_4^{2-}). Water–soluble cations were determined using inductivity coupled plasma (iCAP™ 7000 Plus Series ICP–OES, Thermo Scientific™) [46]. Water–soluble anions, however, were determined using titration method [44]: CO_3^{2-} and HCO_3^- by sulfuric acid (H_2SO_4), Cl^- by silver nitrate ($AgNO_3$) and SO_4^{2-} by versenate solution. Concentration of total organic elements, including C, H, N and S were measured using dry combustion technique by CHNS analyzer (Thermo Scientific Flash 2000) [47]. Meanwhile, total inorganic elements concentration were digested using the mixture of nitric acid (HNO_3,70%) and hydrochloric acid (HCl, 35%) by a Milestone MLS 1200 Mega microwave digestion instrument and determined using ICP [48]. Available concentrations of nitrogen (N), phosphorus (P) and potassium (K) were determined in the soil extraction of 2.0 M potassium chloride (KCl) by an automatic Kjeldahl analyzer (Behr S5), 0.5 M Sodium Bicarbonate ($NaHCO_3$) by a spectrophotometer (T80 UV–Vis, PG Instruments) and 1.0 M ammonium acetate (CH_3COONH_4) by a flame photometer (Sherwood MODEL 360), respectively [49].

2.5. Incubation experiment

A 30–day incubation experiment was conducted in triplicates at constant temperature (25 ±0.5 ^oC) to evaluate the short-term effect of biochar (2.5%

w:w) on P dynamics and transformations in the soil-biochar interface. Soil moisture content was kept constant at the field capacity by application of monobasic potassium phosphate (KH_2PO_4) solution (200 mg L^{-1} P) to ensure that all soil microsites are exposed to the same initial P concentration simultaneously. The moisture content was readjusted through weight loss compensation by the same KH_2PO_4 solution. Soil samples were collected at the end of the experiment for soil visualization and P fractionation. Surface characterization of soil after incubation was carried out using SEM visualization to monitor alterations in soil matrix following biochar application. Aggregate fractions analysis was further performed after 30 days with the same treatments of the aforementioned experiment (without P application) by dry sieving method as illustrated by Okebalama and Marschner [50]. Mean Weight Diameter (MWD) was further calculated according to the following equation:

$$\sum_{i=1}^{n} di\ Wi$$

d_i: is the mean diameter of the openings of two consecutive sieves (mm)

W_i: is the weight ratio of aggregates remained on the sieve

i: is the aggregate fractions (mm)

Finally, P fractionation was carried out based on the protocol of Headly et al. [51] and the modification of Zhang et al. [52].

2.6. Column experiment

A column experiment was carried out at Soils Department, Faculty of Agriculture, Mansoura University, Egypt to study the short-term effect of pristine and modified biochars on P dynamics and phytoavailability in different soil layers of the charosphere. Columns were designed using five polyethylene containers (30 cm height and 7.5 cm diameter) comprising four layers as illustrated in Fig. S1: the water head (5 cm), the rhizospheric soil layer (15 cm), the sand layer for aeration (5 cm), and the drainage layer (5 cm). The soil matrix (1.0 kg, 15 cm) was divided into three layers (5 cm for each). Columns were perforated from the bottom to collect leachates, and the drainage layer of the column (5.0 cm) was filled with washed sand to optimize water movement. Cheesecloth sheets (Egyptian cotton fabric) were placed below the washed sand layer to separate solid particles seepage (e.g. soil, biochar or sand) into leachates. Soil leachates were collected into 68 mL polypropylene digestion vessels (Environmental Express). Three seeds of maize (*Zea mays*, cross cv. Giza 10) were sown in each column. The experiment was implemented in a completely randomized block design with three replicates, comprising five treatments: (i) control (without biochar application) and 4 types of biochar application at 2.5% (w:w) i.e. (ii) OB, (iii) BMB (iv) CHB and (v) BIOB. All treatments were fertilized with P in the form of superphosphate (0.2 g per column) and nitrogen in the form of urea (0.1 g per column). The experiment lasted for 30 days, and maize seedlings were collected for recording growth parameters and biochemical analyses.

Additionally, soil subsamples from different layers were collected for monitoring soil physicochemical analysis and P dynamics.

2.7. Soil phosphorus fractionation

Geochemical P was fractionated in soil samples collected after 30 days from microcosms and soil column layers (0–5, 5–10 and 10–15 cm). One gram of representative subsamples was placed into a 50 mL polypropylene centrifuge tube and extracted sequentially into these fractions: (i) water–soluble fraction using 30 mL of DI water, (ii) exchangeable fraction using 0.5 M Sodium bicarbonate ($NaHCO_3$) at pH value of 8.5, (iii) Fe/Al–P using 0.1M Sodium hydroxide (NaOH), (iv) Ca–P using HCL (1.0 M) and (v) the residual fraction by the acid-digestion using the mixture (1:1) of sulfuric (H_2SO_4)/perchloric acid ($HCLO_4$). Each geochemical fraction was shaken for 16 h at 250 rpm and separated using centrifugation. Geochemical fractions of P in each extraction were determined calorimetrically at the wavelength of 720 nm using ascorbic acid method by PG T80 UV/VIS spectrophotometer.

2.8. Maize seedling measurements

Maize seedlings were harvested 30 days after sowing. Vegetative growth parameters, including plant height, fresh weight and dry weight were recorded. Leaf area of plants was measured according to Francis and coworkers [53]. Plant samples were oven-dried at 70 ^{o}C, digested by the mixture of H_2SO_4/$HClO_4$ acids and subjected to plant nutrients determination: N using Behr S5 automatic Kjeldahl, P using UV/VIS spectrophotometer and K using flame photometer (Sherwood MODEL 360).

2.9. Quality control and statistical analysis

Soil and plant analyses were carried out in ISO/IEC 17025 accredited laboratories under adjusted environmental conditions, including temperature (≃25°C) and humidity (45%), which recorded using a HT–306 HUMIDITY/TEMP METER (±3.5% RH and ±3.0% of rdg + 4 °C digits). Equipment was routinely calibrated to guarantee QA/QC verifications. All chemical reagents (Fisher Scientific) of analytical grade were used to ensure accuracy of analyses. Additionally, ultrapure deionized water (18.2 MΩ) (Nanopure water, Barnstead) was utilized for preparation of chemical solutions. Chemicals and supplies were sterilized at 121 ^{o}C/1.0 bar using a high-pressure steam sterilizer for 15 min during biological preparations. Protocols of soil and subsampling pretreatment was performed according to ISO 11464 standard [54]. In order to minimize the error values, replications, controls and blanks were considered during analytical measurements. Soil water content and dry weight measurements were carried out according to the ISO 11465:1993 standard [55]. A standard material (BBOT STANDARD CHNS; C_{26} H_{26} N_2 SO_2) was purchased from Fisher Scientific for optimizing the determination of organic elements using CHNS analyzer. Additionally, standardized calibrating solutions (Fisher Scientific, R^2 ≥0.99) were used for verification of inorganic elements measurement using ICP. Values of detection limit of inorganic elements (µg L^{-1}) were Al (51.11), B (22.32), Ba (24.33), Cd (50.98), Cr (31.51), Co (35.55), Cu (19.99), Fe (47.10), Hg (24.02), Mn (31.24), Ni (39.58), Pb (54.85), V (26.59) and Zn (40.89). values of

recovery of elemental analysis determination oscillated in the rage of 92.15–105.50%. Normality of the data distribution was verified using Shapiro–Wilk test (p-value). Statistical analysis was carried out based on one–way analysis of variance (ANOVA) with Duncan's multiple range tests at a confidence level of 95% using CoStat software (Version 6.303, CoHort, USA, 1998–2004).

3. Results and discussions

3.1. Biochar characterization

Spectroscopic, physical and chemical properties of pristine and functionalized biochars were characterized according to the standard methods to understand mechanisms responsible for P modulation in each soil type. This intensive characterization might help in developing fit–for–purpose forms of functionalized biochars tailored in improving P phytoavailability in the charosphere of different soil types.

3.1.1. Spectroscopic characterization

3.1.1.1. SEM and EDS analysis

The structural morphology of pristine and functionalized biochars was visualized by SEM as illustrated in Fig. 1A. The surface morphology of pristine biochar (Fig1A, a1) was rough with abundance of marco- and mesopores rather than micropores, which is commonly presented in the surface morphology of most carbonaceous materials [56]. Most of these pores, however, were blocked due to the formation of ash-based minerals during the thermochemical conversion process [57]. SEM micrographs of CHB (Fig1A, a3) exhibited a rough structure with bulges inflammation and bulges formation

due to reconfiguration of the rigid surface of pristine biochar by the erosive action of $KMnO_4$ that caused blocking of pores by excessive minerals impregnation [58]. Ball-milled biochar exhibited an irregular granular-like shape confirming the breaking/crashing of original biochar particles into ultrafine particles (Fig1A, a5). The porosity like shape of BMB was not pronounced in BMB. Presumably, due to formation of the ultrafine particles, which caused blockage of biochar's pores. SEM visualization of BIOB showed the presence of *Bacillus subtilis* in a bacillary-like shape onto biochar surfaces (Fig1A, a7). This evidence confirmed the successful inoculation of biochar given its carbonaceous matrix and porous structure supporting its utilization as a microbial shelter [59]. Besides, biochar particles adhered together through the biofilm formation of extracellular polymeric substances secreted by the niche of microorganisms [60].

Carbon peak was the dominant onto outersphere surfaces of different biochars and ranged between 84.54–88.38%. Elevated peaks of O were also noticeable in different biochar, wherein the highest value (10.04%) was pronounced with BIOB. This is related to aging/oxidation processes caused by active metabolites of B. *subtilis*, which caused grafting of carboxylic and phenolic groups onto BIOB surfaces [61]. Sodium peak showed higher value with OB (0.49%) and vanished completely with CHB given the exchange with Mn^{2+} ions. Meanwhile, a high peak of Mn (0.95%) was clearly noticeable with CHB, which was not observed with other types of biochar. Interestingly, K showed a lower peak with CHB than OB and BMB. This could be attributed

to the easily exchange of K^+ by Mn^{2+} onto outersphere surfaces of biochar during $KMnO_4$ impregnation, taking into consideration the loose hydration shell of K^+ [62]. Unlike other biochars, BIOB showed peaks of P and S. These peaks might be derived from proteins and other metabolites of B. *subtilis* secretion. Besides, the presence of the P peak onto BIOB reflected the high efficacy of B. *subtilis* colony on solubilization of the inherent insoluble phosphate minerals existed in OB (particularly struvite, (NH_4) $MgPO_4.6H_2O$; Table S_2).

3.1.1.2 TGA and DSC analyses

TGA analysis was performed to identify the stability of biochar through decomposition at different temperatures. Distinct phase of weight increases by about 0.233, 0.138 and 0.108% were observed with OB (33.28–54.86 °C), BMB (29.38–45.97 °C), and CHB (38.81–52.14 °C), respectively, due to physisorption of gases at initial stage of thermal decomposition. This initial phase of weight increase, however, was not observed with BIOB. This could be attributed to the higher rate of wight loss induced by the fast decomposition of some microbial metabolites below 100 °C than the weight increases derived from physisorbed gases. The final weight losses of biochar at final temperature degree (620 °C) were respectively 97.03, 92.00, 88.97 and 88.13% with OB, BMB, CHB and BIOB. This finding highlights the high stability of OB relative to other types. Biochar types showed comparable TGA curves with two distinct stages of weight loss (Fig.1B, a and Fig S2). The initial stage of weight loss from pristine and modified biochars *via* thermal

decomposition was respectively 1.39% @ 172 ºC, 2.73% @ 167.75 ºC, 5.12% @ 202.13 ºC and 6.60% @ 130.77 ºC with OB, BMB, CHB and BIOB, which related to moisture evaporation and low molecular weight organic substances volatilization from 100 to 200 °C. These results pointed to the potentiality of functionalized biochars to bind water molecules and low molecular weight organic substances over the pristine form. The second distinct phase of weight loss was recorded at temperatures of 493 °C (OB), 501 °C (BMB), 482 °C (CHB) and 497 °C (BIOB) with weigh losses of 0.470, 0.533, 0.492 and 0.611%, respectively. This obvious phase of weight loss refers to the disintegration of polysaccharides/carbohydrates (above 200 °C), hemicelluloses (220–315 °C), cellulose (315–400 °C), and lignin (up to 620 °C) [63].

Differential Scanning Calorimetry (DSC) thermograms (30–600 °C) were further used to measure the differential heat flow of biochar. Exothermic reactions occur when there is a negative change in enthalpy ($\Delta H < 0$) with a heat energy generation. Endothermic reactions, however, require a heat energy input to enable the reaction to proceed, wherein the enthalpy change is positive ($\Delta H > 0$). In this study, the heat flow during the initial phase was exothermic, which remained until 17.3 min (194 °C), 16.8 min (189.3 °C), 14.0 (161.3 °C) and 17.7 min (197.9 °C) with OB, BMB, CHB and BIOB, respectively (Fig. 1B, b and Fig S3). The highest rate of enthalpy was 2.92, 2.95, 2.25 and 5.42 mW. Mg^{-1} for OB, BMB, CHB and BIOB, respectively. The high carbon content, hydrophobicity and porosity of biochar support its potential self-

heating through the exothermic oxidation of molecular weight organic substances and the microbiological reactions [64]. In this regard, BIOB denotes the highest heat release compared to other biochars through several exothermic biological processes such as oxidation of organic functional groups and water evaporation [65]. Another endothermic phase was observed in all biochars, which showed the highest rate of enthalpy at 523.1 ^{o}C (49.9 min), 584.4 ^{o}C (56.0 min), 587.2 ^{o}C (56.3 min), and 594.1 ^{o}C (57.0 min) with OB (36.9 mW. mg^{-1}), BMB (50.2 mW. mg^{-1}), CHB (45.2 mW. mg^{-1}), and BIOB (23.1 mW. mg^{-1}), respectively, given the endothermic reactions necessarily for hemicelluloses, cellulose, and lignin decomposition.

3.1.1.3 FTIR and XRD analysis

FTIR spectrographs depict a minimal alteration in the pattern of surface functional groups following functionalization process (Fig. 1B, c). Infra–red spectrum showed a broad peak at wavelength of 3418 cm^{-1}, which correspond to hydroxyl stretching group (OH). Another peak was observed at the wavelength range of 2922–2961 cm^{-1}, which attributed to C–H aliphatic group. This peak, however, did not exist in CHB. Meanwhile, a unique Mn–O vibration at wavelength of 518 cm^{-1} was noticeable in CHB given the formation of $MnO_{(\times)}$ following $KMnO_4$ impregnation [66]. Another spectrum was presented at the wavelength of 1571–1580 cm^{-1}, which corresponds to aromatic C=C or C=O stretching vibration functional group. Noticeable bands also existed at wavelengths of 850 –1000 cm^{-1} and 450–500 cm^{-1} linking to CH_2 and PO_4/CO_3/Si-O functional groups, respectively.

Oxygen containing functional groups of dissolved humic substances were more pronounced than their precursors biochar (Fig. S4). Infra–red spectrum showed the presence of O–H stretching group (alcohol group) at region of 3200–4000 cm^{-1}. FTIR spectrographs confirmed the presence of S=O sulfonyl chloride, C–Cl stretching halo-compound, and C–O stretching aliphatic ether groups at wavelength ranges of 1380–1410, 510–850 and 1085 –1150 cm^{-1}, respectively. FTIR spectra indicated the presence of N–H amine (2500–3000 cm^{-1}) and C–N aromatic amine (1266-1342 cm^{-1}) groups with all dissolved humic substances except those derived from CHB. Conversely, only humic substances derived from CHB showed the presence of C=O group at region between 1600 and 1900cm^{-1}. Unique functional groups were also recognized with OB–DOM at wavelength regions of 1513.45–1564.03 cm^{-1} (N-O nitro compound), BIOB–DOM at 1016.24–1300 cm^{-1} (CO–O–CO stretching anhydride), and OB–DOM and BMB–DOM at 414.55 –468.37 cm^{-1} (Cl and CO_3).

X–ray diffractograms showed a low degree of crystallinity for both of OB and BMB (4.56 and 5.72%, respectively) at 2Θ lie between 10 and 24°, which indicate the degree of either amorphicity or crystallinity of cellulosic compounds in biochar (Fig. 1B, d). In contrast, CHB and BIOB exhibited higher degree of crystallinity (12.78 and 13.40%, respectively) due to the chemical aging by either chemical or microbial enzymatic oxidations [67]. XRD pattern (Fig 1B, d and Table S2) of OB showed sharp peaks at Θ lie between 20.82 and 26.60° with d values 4.26 and 3.42 A° corresponding to struvite

($NH_4MgPO_4 \cdot 6H_2O$) and quartz (SiO_2), respectively. The presence of struvite confirmed the potential contribution of functionalized biochar in P nutrition. Other sharp peaks appeared with both of OB and BMB at Θ of 29.4° (d value = 3.04 A°), which corresponded to calcite mineral ($CaCO_3$). Halite mineral also existed in the X–ray diffractogram at Θ = 39.49° with a d value of 2.82 A°. Another exceptional peak appeared with BMB and BIOB corresponding to graphite mineral (C). This peak appeared in BMB at two positions (2Θ = 26.54 and 59.92°) with d values 3.35 and 1.57 A°, respectively. This unique peak of graphite appeared at only one position in BIOB at an angle of 59.92° with a d value of 1.57 A°. The peak of quartz minerals appeared also in BIOB at Θ 26.58° with a d value of 3.342 A°. Chemical modification process caused a presence of unique peaks related to pyrolusite minerals (MnO_2) at 28.39° (d value = 3.14 A°). Ronneburgite ($K_2MnV_4O_{12}$) is another unique mineral that existed onto CHB at Θ 26.69° with a d value of 3.33 A°. Furthermore, another peak appeared at 2Θ 40.55° and 58.66° with d values of 2.22 and 1.57 A°, respectively, that liked with the formation of manganosite (MnO) onto CHB.

3.1.2. Physical and chemical analyses

Values of biochar's specific surface area ($m^2\ g^{-1}$) were ranked as OB (40.91) > BIOB (34.84) > CHB (29.35) > BMB (21.94) as indicated in Table 1. In addition, total pore volume recorded the highest value with BIOB (0.069 $cm^3\ g^{-1}$) followed by OB (0.068 $cm^3\ g^{-1}$) and CHB (0.061 $cm^3\ g^{-1}$); however, BMB recorded the lowest value (0.049 $cm^3\ g^{-1}$). Meanwhile, the pore diameter values of all biochars were comparable (~1.9 nm). It is clearly noticeable that

ball milling process reduced specific surface area by about 46.4% due to the damage of pores and carbonaceous lattice of biochar and formation of new porous planar structure lacking the abundance of pores and high surface area [68]. Likewise, chemical modification process minimized the specific surface area of CHB. Presumably, due to the formation of small particles of $MnO_{(\times)}$, which deposited into the interior pores of biochar to cause blockage of micro pores [69].

pH values of functionalized biochars (Table S3) ranged between 9.21 (OB) and 9.71 (BMB), which depends upon the ash, carbonate and organic/inorganic alkalis content as well as the content of active functional groups (e.g. –COOH and –OH) [70]. Besides, salinity values (expressed as electrical conductivity) varied greatly among types and ranked as BMB (3.18 dS m^{-1}) > CHB (1.05 dS m^{-1}) > BIOB (0.53 dS m^{-1}) > OB (0.491 dS m^{-1}). Ball milling process caused a significant increase in the EC value of BMB due to the enhancement of biochar graphitization [71]. Besides, ball milling might induce higher accessibility/exchangeability of dissolved inorganic cations (e.g. Ca^{2+}, Mg^{2+}, Na^{+}, and K^{+}) [72]. Zeta Potential (ζ) analysis explained the electronegativity of modified and pristine biochars (between –25.6 and –15.3 mV). In this regard, BIOB exhibited the highest value of electronegativity since electroactivity is a cellular character correlated with the metabolic activities of B. *subtilis* [73].

Point of zero charge (pH_{PZC}) values of biochar were respectively 7.5, 7.8, 7.7 and 7.82 for OB, CHB, BMB and BIOB (Fig. S5). These values were below the

pH of the solution. In aqueous solutions with pH values below the pH_{pzc}, biochar is protonated to favor the binding of anionic sorbates by the positively charged surfaces. In contrast, when the pH value of the solution exceeds the pH_{pzc}, the deprotonated negatively charged surface motivates the binding of cationic sorbates through electrostatic attraction forces. These results confirmed the electronegativity of biochar surfaces and their higher tendency toward sorption of cationic sorbates rather than anionic ones. Therefore, the binding capacity of P onto biochar surfaces will not be strong due to the repulsion force between the negatively charged surfaces of sorbent and sorbate as well as the competition between phosphate and hydroxyl ions on the sorption sites of biochar.

Elemental composition of modified and pristine biochars (Table S3) pointed to noticeable differences in total carbon concentration since OB and BMB recorded the higher values (42.22 and 40.26%) than CHB and BIOB (35.51 and 37.19%). Nitrogen showed considerable values in the functionalized biochars (1.69–2.18%). What's more, P concentration in biochars showed relatively higher values (0.59–0.95%) given the high P concentration in *Dodonaea viscose* (the feedstock material). Labile P fractions of biochar comprising soluble (H_2O–P) and exchangeable ($NaHCO_3$–P) values showed considerable increase following functionalization (Fig. S6). In this regard, CHB showed the highest values of soluble (409.46 mg kg^{-1}) and exchangeable P (816.95 mg kg^{-1}); however, OB recorded the lowest values (151.95 and 305.66 mg kg^{-1}, respectively). Potassium concentration ranged between

0.86% (BIOB) and 2.52 (OB). Data of K concentration in CHB (1.96%) was lower than its original form. This finding supports data of EDS analysis. Calcium showed also high values in the functionalized biochars and ranged between 3.84% (CHB) and 4.86% (BIOB). The concentration of Mg was comparable in all biochars with relatively higher value in BIOB (0.92%). Concentrations of micronutrients showed considerable values for plant nutrition: Fe (7375–10003 mg kg^{-1}), Zn (412–522 mg kg^{-1}), Cu (23.85–86.73 mg kg^{-1}). Meanwhile, Mn concentration showed a sharp increase by about 490 folds in CHB over its original form (114.8 mg kg^{-1}) following $KMnO_4$ impregnation. Values of potentially toxic elements (Ba, Cd, Cr, Pb and Ni) were within the safe limits for plant nutrition.

3.2. Changes in Soil phosphorus fractions after incubation

3.2.1. Surface morphology characterization of soil-biochar matrix

SEM visualization imaging after incubation showed a coarser morphology of unamended soil matrix relative to the amended treatments, which became surrounded with biochar particles in a complex matrix (Fig. 2). Biochar particles appeared with a higher aggregated shape with soil particles in CHB amended treatment relative to those amended with OB. This could be attributed to the high functionality of CHB to form organo-mineral complexes with soil matrix. Soils treated with BMB showed the presence of ultrafine particles with few different-sized agglomerates of soil-biochar aggregates. Besides BMB-treated soils (soil a in particular) showed the presence of macrobiotic creatures since the ultra-fine particles of biochar are considered

as a favorable shelter for optimum microbial colonization. Soils treated with BIOB showed the existence of B. *subtills* colony in soil matrix confirming the successful biological activation process. In addition, soil-biochar aggregates appeared in a smooth-like shape with vanishing of the common features of biochar particles. This is mainly attributed to the secreted extracellular polymeric substances, which could act as a sticky material for soil-biochar aggregation.

EDS spectra of unamended soils (Fig. S7) showed elevated peaks of O (50.93–68.88%), Si (15.62–25.24%) and Al (5.30–9.54%) given the anionic Si–O–Al linkages of aluminosilicates in soil. Soil b showed a high peak of Ca (6.95%) confirming its high $CaCO_3$ content compared with lower Ca peaks with soils a (2.52%) and c (1.35%). This finding was consistent with the gasometric determination of $CaCO_3$, which showed higher value with soil b (12.5%) relative to soil a and c that showed comparable values of $CaCO_3$ (3.2 and 2.9%, respectively). High peaks of O, Si, Al and Ca showed significant declines following biochar application with presence of high C peaks (58.61–72.30%) confirming the exterior coating of biochar to soil granules. In this regard, C peaks showed the highest values with BMB (60.54–69.99%) and BIOB (61.39–76.94%). These high peaks of C with BMB confirmed the high ability of nano biochar particles to form smooth surfaces onto soil particles. Additionally, the high C peaks with BIOB might be attributed to the biofilm formation of extracellular polymeric substances secreted by the niche of B. *subtilis*, which could generate a sticky material to bind biochar onto soil

surfaces. Soils amended with CHB showed the presence of Mn, which might provide an important source of plant nutrition. The elevated peaks of Ca and Fe onto the unamended soils (1.35–6.95% and 3.20–7.73%, respectively) declined sharply following biochar incorporation. This important finding highlights the importance of biochar to reduce the dominance of Ca and Fe ions onto outersphere surfaces of soil matrix. Accordingly, minimize their negative effects on phosphate fixation/precipitation.

3.2.2. Aggregate fractions after soil incubation

Biochar amended soils showed reductions in macroaggregate fraction (2–0.25 mm) by about 4–8% relative to the unamended ones (Table 2). Presumably, due to the relatively short-term effect of soil incubation (30 days), which is not sufficient to form stable complexes between soil and biochar surfaces [74]. Besides, the low pyrolysis temperature (< 550 ^{o}C) is mainly associated with a lower beneficial effect on soil aggregation since the high pyrolysis temperature (> 550 ^{o}C) increases the biochar's hydrophobicity. This hydrophobic nature of biochar might lessen the dispersion of soil aggregates and reinforces the organo-mineral complexes formation between soil and biochar particles [75]. Conversely, functionalized biochars showed an opposite trend for microaggregate fractions formation (<0.25–0.05 mm) with increases by about 7.75 and 37.37%. This means that most of the applied biochar was distributed in microaggregate fractions (< 0.25–0.05 mm) during this short incubation period [74]. Microaggregates are the most stable soil fraction unit, which composed from integration of organic mineral and

bioactive compounds, that could provide habitats for biodiversity of organisms involved in nutrient cycling in the rhizosphere. Further to this, it was reported that the phytoavailable P forms tend to accumulate in the microaggregates fraction of soil matrix [76]. The accumulation of biochar in the microaggregates fraction might act as a safeguard against phytoavailable P fixation through reducing the reaction of orthophosphates with calcium carbonate, iron (Fe) and aluminum (Al) (oxyhydr)oxides. Original biochar showed the highest increments in microaggregates fraction in soils a and b (32.85 and 8.08%, respectively); however, BMB showed the highest motivating effect for increasing microaggregates fraction in soil c (37.37%). Other biochars (BMB and BIOB), however, showed an opposite trend with soil b since there was no obvious alteration in microaggregates fraction (0.64 and 0%, respectively) with a noticeable increase in macroaggregate fraction (7.67 and 12.64%, respectively). There are two reasons that might justify this noticeable trend, firstly: ball milling technique generated more fine biochar particles with higher total surfaces to provide more sorption sites for combination with cementing cations (e.g. Ca^{2+} and Mg^{2+}) for effective macroaggregates formation [77]. Secondly, the secretion of adhesive materials from microorganisms underlines the ability of BIOB to form consistent macroaggregates with fine particles of $CaCO_3$ existed in soil b. Soil biochar applications might enhance MWD due to its high content of TOC, which increases the hydrophobic nature and adhesion among soil particles. In the current study, however, biochar has no effect on MWD given the short

duration, which was insufficient to form large stable aggregates following biochar application. **To sum up, biochar tends to accumulate in the microaggregates fraction of soil (the sink of soil P), leading to safeguard orthophosphates against fixation by reaction with active soil components (e.g. $CaCO_3$, Fe/Al (oxyhydr)oxides.**

3.2.3. Phosphorus fractionation

The distribution of soil P concentration (mg kg^{-1}) and fractions as a percentage of total content was presented in Table S4 and Fig. 3, respectively. The labile phosphate pool (water soluble and exchangeable fractions) showed variable values among treatments with higher value with soil a (52.32 mg kg^{-1}) and lower values with soil b (13.23 mg kg^{-1}) and c (27.72 mg kg^{-1}). The moderately labile fraction (Fe/ Al–P) was comparable with soils a and c (47.04 and 45.68 mg kg^{-1}) and very low with soil b (4.79 mg kg^{-1}). The majority of P-fractionated pool was dominant in Ca–P fraction (the low labile pool) given the high content of Ca in arid and semi-arid soil conditions. The residual P fraction recorded the highest value in soil c (285.39 mg kg^{-1}). The non-labile P fraction is strongly bound or chemically fixed with the dominant secondary minerals (calcite) with less phytoavailability potential.

Biochar application led to a significant increment in the labile P pool including soluble and exchangeable fractions. This increase in phytoavailable P is mainly associated with the direct effect of P inputs derived from biochar as well as the indirect effect associated with the modulating effect of biochar

on legacy P. Increments of water-soluble P varied among different soil types and reached ranges of 85.74–218.13%, 53.86–870.25%, and 354.79–557.68% with soils a, b and c, respectively. Exchangeable P also showed significant increments in soil a (92.71–154.89), b (515.51–982.92%) and c (205.86–303.29%) following biochar application. Ball milled biochar exhibited the highest efficacy for improving solubility of soil P. Presumably, due to increasing soil wettability following BMB application, which in turn maximized the solubility potential of phytoavailable P. According to Zhao et al.'s study, there are certain amounts of phytoavailable P release following ball milling process [78]. In view of this, biochar pyrolyzed at low temperatures showed higher wettability potential than those produced at higher temperatures (> 600 ^{o}C) [79]. Additionally, ball milling process could effectively promote the interaction between generated submicron particles of biochar and applied P through active functional groups in forms of P–O/P=O and C–O–PO_3 against precipitation onto soil particles [28]. Biologically activated biochar showed the highest performance for improving P phytoavailability relative to other modification techniques in soil b (114.37 mg kg^{-1}). Meanwhile, it recorded the highest performance after BMB with soils a and c (123.6 and 71.34 mg kg^{-1}). This could be attributed to the mobilization of legacy P by organic acid secretion (e.g. citric and oxalic acids) and soil phosphatase associated with bacterial activity of BIOB [80]. On the other hand, the superiority of BMB in soils a and c highlights the efficiency of ball milling process on liberating phytoavailable P in soils containing considerable

amounts of clay minerals. The highest clay content was recorded with soil a (31.5%) with lower value in soil b (28.2%) and minimal value in soil c (8.0%). The existence of considerable clay fraction content in the root zone could accelerate P phytoavailability from active components trapped into clay plates (e.g. sesquioxide, calcium carbonate and organic matter) [81]. Nevertheless, the relatively considerable clay fraction content in soil b is mainly derived from fine particles of active calcium carbonate, which have a significant effect on orthophosphates precipitation. A remarkable increase of Fe/Al–P was observed with soils a and b following BIOB application (64.07 and 14.91 mg kg^{-1}). This might be related to the instantaneous acidification effect generated from organic acid secretion (e.g. oxalic acid) by loaded bacteria, which might liberate Fe and Al ions following the dissolution of Fe/Al–oxides [82]. Additionally, B. *subtilis* inocula may secreted various active compounds capable of chelating Fe and Al ions, thereby orthophosphates can be liberated from surfaces of sesquioxides [83]. Conversely, a negligible reduction in this fraction was observed in all soil types following CHB application. This might be related to the inherent $MnO_{(\times)}$ of CHB generated following $KMnO_4$ impregnation, which could form complexes with orthophosphates [27]. A slight increase was observed in the non-labile P pool (Ca- and residual P fractions) compared to the labile one (soluble and exchangeable fractions) with all amended biochar soils given the abundance of Ca^{+2} in all soil types, which is the main reason for P precipitation in the non-labile P pool. **In essence, BMB exhibited superior performance in**

enhancing labile P fractions by improving soil wettability and forming complexes through its active functional groups, thereby reducing P fixation. BIOB, however, ranked following BMB in labile P solubilization through the secretion of microbial exudates that increase P solubilization.

3.3. Vertical redistribution and plant uptake in the column experiment

3.3.1. Effect of biochar addition on soil pH and EC

Soil reaction varied between weakly alkaline in soil a (pH=7.84) and moderately alkaline in soils b and c (8.18 and 8.09, respectively; Table 3). It is worth noting that soil pH value is crucial for modulating the dissolution of soil P since the high pH could promote the release of NaOH–P (Fe/Al–P) through the ligand exchange reactions between OH^- ions and orthophosphate [84]. Conversely, the low pH value could accelerate the release of Ca–P. A noticeable decline in soil pH values was observed in subsurface layers (5–10 and 10–15 cm) relative to the surface ones (0–5 cm). This could be attributed to the upward movement of soil solution through capillary action, wherein less soluble salts (carbonate in particular) were accumulated in the surface layer following water evaporation. Additionally, root exudation and respiration might cause a proportion decline in soil pH value of the rhizospheric layer. In view of this, the release of charges carried by H^+ to compensate cations taken up by plants and the secretion of acidifying compounds (e.g. citric acid, malic acid, and oxalic acid) might cause a decline

in soil pH value [85]. Further to this, root respiration might result in a build-up of CO_2 in the root zone, which might dissociate in the alkaline soil to cause a decline in soil pH value.

Biochar showed contradictory results in pH value of different soil layers and types (Table S5 and Fig. 4). A noticeable reduction in pH value was recorded in different layers of soil a (0.13–0.21 units) following biochar application with a slight increase with BMB (up to 0.1 units). This reduction in soil pH value could be attributed to the production of acid compounds generated from oxidizable composites of biochar by chemical/microbial decomposition (particularly in the surface layer) [86]. For instance, several chemical/microbial-oxidizable compounds (e.g. alcohols, polysaccharides and anhydro-cellulose) could be existed in pyrolyzed biochars at relatively low pyrolysis temperatures [87]. Besides, the presence of biochar in soil matrix might promote the oxidation of soil organic matter to produce acidic compounds involved in reducing soil pH value through its catalytic effect in various oxidation processes [88]. On the other hand, the abundance of alkaline cations (e.g., Ca^{2+}, Mg^{2+}, Na^{+} and K^{+}) held onto soil colloidal phase, especially onto soil b, might exchange with H^{+} generated from complicated reactions among soil-biota-plant system, leading to minimizing the change of soil pH. Besides, the high alkalinity of biochar and its modulating effects on dissolution of alkaline cations (particularly in soil b) might cause an increase in soil pH. It is clearly noticeable that BMB application showed a superiority for increasing soil pH in soil layers/types (8.46 as an average value in different soils). This

finding is consistent with data of biochar analysis, which pointed to high values of EC (3.18 dS m^{-1}), pH (9.71) and sodium concentration (0.75%). Additionally, the high accessibility/exchangeability of inorganic cations (e.g., Ca^{2+}, Mg^{2+}, Na^{+}, and K^{+}) might cause an incremental rise in soil pH. Conversely, CHB application was associated with the lowest soil pH value (8.29 as an average value in different soils). This could be attributed to the acidifying effect of manganese chloride, which generated following Mn discharge from CHB [89].

Soil salinity values varied among different types, wherein soils b and c were slightly saline (1.32 and 1.61 dS m^{-1}, respectively) and soil a was moderately saline (2.57 dS m^{-1}). The relatively high EC value of soil a could be attributed to the secondary salinization derived from the inappropriate drainage in soil. A gradual increase in soil salinity was observed in subsurface layers relative to surface ones due to the vertical migration of soluble salts with the vertical movement of applied water. This increase of soil salinity reached 25–165.38, 19.14–225.23 and 3.23–9.67% with soils a, b and c, respectively. Salinity-induced ionic strength showed a high modulating effect on phytoavailability of orthophosphates [90]. Although the salinity value of BMB was higher than other biochars, its application caused a decline in soil salinity by about 32.25, 6.38, and 30.3% with soils a, b and c, respectively. The distribution of fine BMB particles into soil matrix might reduce the vertical velocity flow of water within soil layers, leading to better dislodging salts from the charosphere [91]. Furthermore, the high sorptivity of BMB might precipitate multiple soluble

ions (e.g. Na^+, Ca^{2+}, K^+ and Mg^{2+}) *via* several chemisorption mechanisms [92]. **In brief, functionalization of biochar is urgently needed to mitigate the high alkalinity of arid soils. In addition, biochar application can accelerate the vertical migration of soluble salts through the soil matrix along with downward water movement.**

3.3.2. Available nutrients retained in soil after harvesting

Values of soil available P varied in their adequacy to sustain P supply requirement of plants and varied between sufficient in soil a (39.40 mg kg^{-1}) and very low in soils b and c (2.90 and 5.60 mg kg^{-1}, respectively; Table 3). Phytoavailable P showed considerable increase in biochar amended soils after maize cutting (Fig. 5). This is mainly related to: (i) the direct effect of considerable P derived from biochar application, (ii) the modulating effect of biochar on soil P dynamics in the charosphere and, (iii) the ability of biochar to minimize the affinity between phosphate and active soil constitutions responsible for phosphate precipitation (e.g. calcium carbonate and clay minerals) [93]. These increases reached 110.51, 92.04 and 184.93% with soils a, b, and c, respectively (Fig. 5). The highest value of available P (115.32 mg kg^{-1}) in soil a was recorded with OB followed by BIOB and CHB. However, the lowest values were comparable with BMB and the control (57.06 and 54.78 mg kg^{-1}). This low available value with BMB could be attributed to the migration of P within ultrafine particles of BMB. Likewise, available P decreased in soil b from 44.12 with control to 37.44, and 43.7 mg kg^{-1} with BMB and BIOB, respectively. However, CHB recorded the highest value

(84.73 mg kg^{-1}) among all treatment. The relatively lower electronegativity of CHB might increase phosphate binding relative to other forms. In this regard, data of XRD demonstrated the successful loading of multiple manganese oxides, including manganosite, pyrolusite and ronneburgite with positive surface charges able to attract orthophosphates. Data of FTIR also pointed to the presence of the unique Mn–O vibration bond, which can form $Mn–PO_4$ complexes with phosphates. Likewise, the presence of C=O group in humic substances derived from CHB pointed to its importance in orthophosphates sorption given its polarity, potential participating in hydrogen bonding, and its participation in several chemical reactions. What's more, $MnO_{(\times)}$ loading onto CHB could generate amphoteric sites onto CHB surface with a high potential for generating negatively charged surfaces at alkaline conditions [69]. Additionally, the relatively low P concentration in maize seedlings might give insights regarding available P retained in soil after harvesting. Available P retained in soil c showed also higher values relative to the control treatment with a noticeable superiority to BIOB (75.82 mg kg^{-1}). This could be attributed to absence of active soil constitution responsible for binding of phytoavailable phosphate, such as the high content of calcium carbonate in soil b and clay minerals in soil a. Consequently, phytoavailable phosphate was bound onto BIOB against fixation by soil constitutions.

Soil available N (Table 3) showed high value in soil a (110.95 mg kg^{-1}) due to the continuous application of mineral N fertilizers. Meanwhile, available N content varied between low in soil b (21.42 mg kg^{-1}) and medium in soil c

(57.8 mg kg^{-1}). Available N showed higher concentrations in soils amended with biochar in comparison with the unamended ones after maize harvesting. This is mainly related to the high functionality of biochar responsible for maximizing N use efficiency through increasing N inputs derived from its inherent N content (1.69–2.18%) and stimulating activities of microorganisms responsible for nonsymbiotic biological N fixation (28.1% increase over the unamended treatments) as well as reducing N losses associated with runoff/leaching and volatilization/emission [15]. Data of soil available nutrients (Table 3) illustrated that K was sufficient in soils a and b (565.45 and 407.59 mg kg^{-1}, respectively) and insufficient in soil c (169.49 mg kg^{-1}). The high potassium content in soil b is mainly associated with the prevalence of K-containing minerals (e.g. glauconite) in Minia location [94]. Unlike available concentrations of N and P, available K showed the highest values in OB amended soils with increments of about 160.77, 107.16 and 146.61%, with soils a, b and c, respectively. This is mainly related to the high content of inherent potassium in the pristine biochar form. Additionally, the higher uptake of K by plants grown under soils amended with functionalized biochars might reduce the final concentration of available K retained in soil after harvesting. **In short, biochar application enhances P phytoavailability in soil *via* its inherent P content, its modulating effects on P dynamics and its ability to minimize the affinity between orthophosphates and active soil components responsible for P**

fixation. Biochar can also stimulate the phytoavailability of N and K by supplying these nutrients from its intrinsic composition.

3.4. Implications for P Bioavailability

3.4.1. Effect of biochar application on soil P fractionation in different soil layers

Hedley's sequential extraction technique was adopted to understand the effect of pristine and functionalized biochars application on soil P dynamics in different layers of maize's charosphere. Labile P pool (water soluble and exchangeable forms) showed an enhancement in response to biochar application (Fig. 6). Regarding P fractions in soil a, it seems that CHB showed a superiority for enhancing the labile P pool in the first layer (0–5 cm); however, the pristine biochar exhibited the highest contribution for increasing this labile P form in subsurface layers (5–10 and 10–15 cm). Although BMB showed the superiority for increasing the labile P pool in the incubation experiment, CHB was superior in the biological experiment. This might be related to the formation of colloidal films from manganese oxides onto fine root hairs, with high ability to stably adsorbed onto these colloidal films [95]. In the subsurface layers, however, it seems that humic substances derived from OB were crucial for increasing the labile P form through increasing phosphate dissolubility. The chemically modified biochar seems to have an encouraging effect for increasing the content of Fe/ Al–P given the ability of $MnO_{(\times)}$ to bind metal(loid) ions (e.g. Fe and Al) and thus liberating phosphate bound onto sesquioxides. The highest residual P fraction was

recorded with the unamended treatment; however, BMB recorded the lowest residual fraction with a decline by about 24% than the unamended treatment. A remarkable increase in the labile P pool was recorded in the surface layer of soil b taking into consideration the beneficial effect of root exudates on solubilizing precipitated phosphates in alkaline and calcareous soils [96]. It is clearly noticeable that CHB was the superior treatment for maximizing the labile P pool in soil b although BIOB showed superiority in the incubation experiment (Table S6). According to Wang and coworkers, maize roots are able to generate phosphatase into the rhizosphere for effective mineralization of organic P [28]. Authors also illustrated that maize roots promoted the colonization of effective bacteria (Saccharibacteria) capable of secreting phosphatase to the rhizosphere. Therefore, the colloidal manganese oxide particles might provide an adsorbent surface for phosphatases [97]. The behavior of CHB in maximizing the moderately labile fraction (Fe/ Al–P) was also remarkable in soil b. The Ca–P was the dominant fraction in soil b with lower values than other soils, given the low solubility of calcium ions in soil b. This fraction showed higher values in OB amended soil as compared with other treatments. These findings suggested that CHB exhibited higher efficacy in increasing labile P pool relative to other biochars, particularly in calcareous soil. This could be attributed to the positive effect of CHB on modulating soil pH, colloidal films formation onto fine root hairs from manganese oxides and its ability to bind metal(loid) ions, thereby liberating phosphate bound onto sesquioxides.

Unlike the superiority of BMB on enhancing the labile P pool in soil c, BMB exhibited higher efficiency under the column treatment with increments by about 132.95, 56.19, and 175.99% for layers 0–5, 5–10 and 10–15, respectively due to its high efficiency in phosphatases excretion. The moderate labile fraction was comparable in soil c layers although OB and CHB showed higher values than other treatments. Ca–P fraction dominated in soil c with a notable superior to the OB treatment. Likewise, OB was the superior treatment for enhancing the residual fraction in soil c.__**To summarize, biochar application shows a stimulatory effect on enhancing labile P pool (water soluble and exchangeable forms). In this regard, root exudates play prominent role in motivating solubilization of precipitated phosphates in alkaline and calcareous soil.** Modulating mechanisms underlying P availability by functionalized biochars are summarized in Table S7.

3.4.2. Vegetative growth parameters and nutrients concentration in maize seedlings

Plants grown under amended soils showed contradictory results in their vegetative characters, including plant height, longest leaf, leaf area, and fresh/dry weight yields (Table 4). Physically and biologically activated biochar showed a high superiority for improving vegetative growth parameters (fresh and dry weight in particular). BIOB recorded the highest value for longest leaf in soil c with an increasing rate up to 28.89%. Meanwhile, it comes in the

second rank after BMB for fresh weight, dry weight, plant height, and leaf area with increasing rate up to 85.87, 229.31, 33.33 and 47.41%, respectively. This could be attributed to the ability of BIOB to modulate soil physicochemical characteristics in such soil conditions and the high efficacy of B. *subtilis* inocula to flourish as endophytes in such soil conditions. Chemically activated biochar showed a superiority for improving vegetative growth characters of maize seedlings grown in soil b due to the high electron shuttling capacity of MnO–biochar in lowering N_2O emissions from soil denitrification [98] and improving plant growth and development through inspiring physiological plant process (e.g. lateral root growth, proteins synthesis, and H^+–ATPase activity) [99].

Original and functionalized biochars showed a high increase in P concentration in maize seedlings over the unamended treatments. This increase ranged between 12.5–56.25, 54.54–90.91, and 7.14–14.28% for soils a, b and c, respectively. Several reports suggested the low desorbability and bioavailability of sorbed phosphate onto biochar surfaces [100-102]. Therefore, it is highly recommended to adopt utilization of biochars derived from feedstock with a high P content and low phosphate sorptivity in order to maximize phosphate desorbability and recyclability. As mentioned earlier, the direct effect of inherent P content and the indirect effects of biochar on modulating phosphate dynamics in the charosphere participated mutually in improving the phytoavailability of P. The biologically activated biochar showed a high superiority for maximizing orthophosphate uptake from the charosphere

through production of solubilizing organic acids and/or phytase enzymes. Furthermore, protons secretion, which associated with microbial metabolism, might cause instantaneous acidifying effect in the charosphere, which in turn increased phytoavailability of P and its uptake by plants [103]. The unique properties of biochar, including its porous structure, outstanding water holding capacity, plethora of active functional groups and considerable nutrients content, participated together to favor the effective adhesion and proliferation of B. *subtilis* inocula. Additionally, recent reports suggested the entrapment of P derived from biochar by phosphate solubilizing bacteria in the form of polyphosphate rather than interaction with soil components in precipitated apatite forms [31].

Unlike P, biochar application didn't affect N concentration in both soil (a) and (c) compared to the control; however, biochar application significantly increased N concentration in soil b by about 2.21–141.91%. Chemically modified biochar recorded the heights value followed by BMB and OB. This increment may be due to the ability of biochar to lessen N loss from calcareous soil *via* sorption of NH_4^+ ions on its surface, leading to prevent their microbial transforming into NO_3^- ions [104]. It was also reported that biochar was able to improve N assimilation through motivating activities of several soil enzymes involved in this mechanism, including nitrate/nitrite reductase and glutamate/glutamine synthetase [105]. Potassium concentration showed also high values in maize seedlings with response to biochar application with a superiority to BMB. The considerable concentration of K in

biochars (0.86–2.28) might provide a steadily supply for potassium nutrition. Additionally, the electronegativity and sorptivity of biochar might reduce potassium leaching from the rhizosphere. **In essence, it is important to functionalize fit-for-purpose biochars tailored to specific soil types to enhance nutrient uptake (particularly phosphorus) and improve plant biomass yield.**

4. Conclusion

Functionalizing biochars with less binding forces and efficient modulating mechanisms is urgently needed to unlock legacy P and minimize orthophosphates precipitation in alkaline and calcareous soils. In the current study, *Dodonaea Viscosa* was chemically, physically and biologically functionalized to prepare fit–for–purpose forms of efficient biochars tailored in improving P phytoavailability in alkaline and calcareous soils. The short-term effect of functionalized biochars was studied in both of soil-biota and soil-biota-plant systems. Functionalized biochars exhibited high efficiency in transforming considerable amounts of residual P fractions into labile forms due to several mechanisms responsible for liberating phytoavailable P from soil matrix. The exterior coating of functionalized biochars to particles of alkaline/calcareous soils reduced the affinity between phytoavailable orthophosphates and active soil constitutions (calcium compounds in particular) responsible for their precipitation into unavailable phosphate. Consequently, application of functionalized biochar might contribute to

improve P use efficiency of phosphatic fertilizers and maximize phytoavailability of legacy phosphate. Future research should highlight P dynamics in aggregate fractions of the charosphere to optimize agricultural practices following biochar application.

Acknowledgements

This research was supported by the Mansoura University Research Fund (grant number MU-Agr-21-6). Authors would like also to acknowledge partial support provided by Academy of Scientific Research and Technology (Project ID: 14213). Finally, open access funding provided by Science, Technology & Innovation Funding Authority (STDF) in cooperation with The Egyptian Knowledge Bank (EKB) is gratefully acknowledged.

Conflict of interest (Declaration of interests):

The authors declare no potential conflict of interest. The authors declare that they have no known competing financial interests or personal relationships that could have appeared to influence the work reported in this paper.

Data availability

All data generated by this study are included in this manuscript. Any additional requests for information can be directed to the corresponding author

References

1 Alshaal, T. *et al.* The rhizosphere and plant nutrition under climate change. 275-308 (2017).

2 He, X. *et al.* Global patterns and drivers of soil total phosphorus concentration. *Earth System Science Data* **13**, 5831-5846 (2021).

3 Wang, C. *et al.* The wetter the better? Preferences in plant-microbial competition for phosphorus sources in rice cultivation under contrasting irrigation. *Soil Biology and Biochemistry* **191**, 109339, doi:https://doi.org/10.1016/j.soilbio.2024.109339 (2024).

4 Carreira, J. A., Viñegla, B. & Lajtha, K. Secondary CaCO3 and precipitation of P–Ca compounds control the retention of soil P in arid ecosystems. *Journal of Arid Environments* **64**, 460-473, doi:https://doi.org/10.1016/j.jaridenv.2005.06.003 (2006).

5 Bindraban, P. S., Dimkpa, C. O. & Pandey, R. Exploring phosphorus fertilizers and fertilization strategies for improved human and environmental health. *Biology and Fertility of Soils* **56**, 299-317, doi:10.1007/s00374-019-01430-2 (2020).

6 Khan, K. S. *et al.* Co-application of organic amendments and inorganic P increase maize growth and soil carbon, phosphorus availability in calcareous soil. *Frontiers in Environmental Science*, 1452 (2022).

7 Yang, Z. *et al.* Intercropping regulation of soil phosphorus composition and microbially-driven dynamics facilitates maize phosphorus uptake and productivity improvement. *Field Crops Research* **287**, 108666, doi:https://doi.org/10.1016/j.fcr.2022.108666 (2022).

8 Weih, M., Westerbergh, A. & Lundquist, P.-O. in *Plant Macronutrient Use Efficiency* (eds Mohammad Anwar Hossain *et al.*) 31-44 (Academic Press, 2017).

9 Pavinato, P. S. *et al.* Revealing soil legacy phosphorus to promote sustainable agriculture in Brazil. *Scientific Reports* **10**, 1-11 (2020).

10 Jalali-Jivan, M., Garavand, F. & Jafari, S. M. Microemulsions as nano-reactors for the solubilization, separation, purification and encapsulation of bioactive compounds. *Advances in Colloid and Interface Science* **283**, 102227, doi:https://doi.org/10.1016/j.cis.2020.102227 (2020).

11 Zhang, X. *et al.* Organic amendments increase crop yield while mitigating greenhouse gas emissions from the perspective of carbon fees in a soybean-

wheat system. *Agriculture, Ecosystems & Environment* **325**, 107736, doi:https://doi.org/10.1016/j.agee.2021.107736 (2022).
12 Gworek, B., Kijeńska, M., Wrzosek, J. & Graniewska, M. Pharmaceuticals in the Soil and Plant Environment: a Review. *Water, Air, & Soil Pollution* **232**, 145, doi:10.1007/s11270-020-04954-8 (2021).
13 Liu, T. *et al.* Measurement of cow manure compost toxicity and maturity based on weed seed germination. *Journal of Cleaner Production* **245**, 118894, doi:https://doi.org/10.1016/j.jclepro.2019.118894 (2020).
14 Liu, X.-P. *et al.* Increased risk of phosphorus and metal leaching from paddy soils after excessive manure application: Insights from a mesocosm study. *Science of the Total Environment* **666**, 778-785 (2019).
15 Ahmad, Z., Mosa, A., Zhan, L. & Gao, B. Biochar modulates mineral nitrogen dynamics in soil and terrestrial ecosystems: A critical review. *Chemosphere* **278**, 130378 (2021).
16 Nahidan, S. & Ghasemzadeh, M. Biochemical phosphorus transformations in a calcareous soil as affected by earthworm, cow manure and its biochar additions. *Applied Soil Ecology* **170**, 104310, doi:https://doi.org/10.1016/j.apsoil.2021.104310 (2022).
17 Khadem, A. & Raiesi, F. Response of soil alkaline phosphatase to biochar amendments: Changes in kinetic and thermodynamic characteristics. *Geoderma* **337**, 44-54, doi:https://doi.org/10.1016/j.geoderma.2018.09.001 (2019).
18 Zhang, X., Li, H., Li, M., Wen, G. & Hu, Z. Influence of individual and combined application of biochar, Bacillus megaterium, and phosphatase on phosphorus availability in calcareous soil. *Journal of Soils and Sediments* **19**, 3688-3698, doi:10.1007/s11368-019-02338-y (2019).
19 Fathy, R., Elagroudi, W., Taha, A. A. & Mosa, A. Modulating effects of biochar on phosphorus dynamics in soil–biota–plant system: a comprehensive review. *Soil Ecology Letters* **7**, 1-32 (2025).
20 Liu, Y. *et al.* Mechanisms of rice straw biochar effects on phosphorus sorption characteristics of acid upland red soils. *Chemosphere* **207**, 267-277, doi:https://doi.org/10.1016/j.chemosphere.2018.05.086 (2018).
21 Chen, W., Ding, S., Lin, Z., Peng, Y. & Ni, J. Different effects of N2-flow and air-limited pyrolysis on bamboo-derived biochars' nitrogen and phosphorus release and sorption characteristics. *Science of The Total Environment* **711**, 134828, doi:https://doi.org/10.1016/j.scitotenv.2019.134828 (2020).
22 Hemati Matin, N. *et al.* Almond and walnut shell-derived biochars affect sorption-desorption, fractionation, and release of phosphorus in two different soils. *Chemosphere* **241**, 124888, doi:https://doi.org/10.1016/j.chemosphere.2019.124888 (2020).
23 Alorabi, A. Q. & Azizi, M. Effective removal of methyl green from aqueous environment using activated residual Dodonaea Viscosa: equilibrium, isotherm, and mechanism studies. *Environmental Pollutants and Bioavailability* **35**, 2168761 (2023).
24 Yaqub, A., Syed, S. M., Ajab, H. & Zia Ul Haq, M. Activated carbon derived from Dodonaea Viscosa into beads of calcium-alginate for the sorption of methylene blue (MB): Kinetics, equilibrium and thermodynamics. *Journal of Environmental Management* **327**, 116925, doi:https://doi.org/10.1016/j.jenvman.2022.116925 (2023).

25 Ai, D., Ma, H., Meng, Y., Wei, T. & Wang, B. Phosphorus recovery and reuse in water bodies with simple ball-milled Ca-loaded biochar. *Science of The Total Environment* **860**, 160502, doi:https://doi.org/10.1016/j.scitotenv.2022.160502 (2023).

26 Zhang, P. *et al.* Amelioration effects of coastal saline-alkali soil by ball-milled red phosphorus-loaded biochar. *Chemical Engineering Journal* **431**, 133904, doi:https://doi.org/10.1016/j.cej.2021.133904 (2022).

27 Che, N. *et al.* Adsorption of phosphate onto agricultural waste biochars with ferrite/manganese modified-ball-milled treatment and its reuse in saline soil. *Science of The Total Environment* **915**, 169841, doi:https://doi.org/10.1016/j.scitotenv.2023.169841 (2024).

28 Wang, S. *et al.* Biochar-seeded struvite precipitation for simultaneous nutrient recovery and chemical oxygen demand removal in leachate: From laboratory to pilot scale. *Frontiers in Chemistry* **10**, 990321 (2022).

29 Chen, W., Wu, Z., Liu, C., Zhang, Z. & Liu, X. Biochar combined with Bacillus subtilis SL-44 as an eco-friendly strategy to improve soil fertility, reduce Fusarium wilt, and promote radish growth. *Ecotoxicology and Environmental Safety* **251**, 114509, doi:https://doi.org/10.1016/j.ecoenv.2023.114509 (2023).

30 Bolan, S. *et al.* The potential of biochar as a microbial carrier for agricultural and environmental applications. *Science of The Total Environment* **886**, 163968, doi:https://doi.org/10.1016/j.scitotenv.2023.163968 (2023).

31 Liu, Z. *et al.* Phosphate-solubilizing microorganisms regulate the release and transformation of phosphorus in biochar-based slow-release fertilizer. *Science of The Total Environment* **869**, 161622, doi:https://doi.org/10.1016/j.scitotenv.2023.161622 (2023).

32 Kumar, M. *et al.* Ball milling as a mechanochemical technology for fabrication of novel biochar nanomaterials. *Bioresource Technology* **312**, 123613, doi:https://doi.org/10.1016/j.biortech.2020.123613 (2020).

33 El-Banna, M. F. *et al.* Sorption of lead ions onto oxidized bagasse-biochar mitigates Pb-induced oxidative stress on hydroponically grown chicory: Experimental observations and mechanisms. *Chemosphere* **208**, 887-898, doi:https://doi.org/10.1016/j.chemosphere.2018.06.052 (2018).

34 Feng, F. *et al.* Use of Bacillus-siamensis-inoculated biochar to decrease uptake of dibutyl phthalate in leafy vegetables. *Journal of Environmental Management* **253**, 109636, doi:https://doi.org/10.1016/j.jenvman.2019.109636 (2020).

35 Ma, X. *et al.* Study of biochar properties by scanning electron microscope–energy dispersive X-ray spectroscopy (SEM-EDX). *Communications in soil science and plant analysis* **47**, 593-601 (2016).

36 Sinha, P. *et al.* Surface area determination of porous materials using the Brunauer–Emmett–Teller (BET) method: limitations and improvements. *The Journal of Physical Chemistry C* **123**, 20195-20209 (2019).

37 Dutta, A. Fourier transform infrared spectroscopy. *Spectroscopic methods for nanomaterials characterization*, 73-93 (2017).

38 Iwashita, N., Park, C. R., Fujimoto, H., Shiraishi, M. & Inagaki, M. Specification for a standard procedure of X-ray diffraction measurements on carbon materials. *Carbon* **42**, 701-714 (2004).

39 Leifeld, J. Thermal stability of black carbon characterised by oxidative differential scanning calorimetry. *Organic Geochemistry* **38**, 112-127 (2007).

40 Fadeeva, V. P., Tikhova, V. D. & Nikulicheva, O. N. Elemental analysis of organic compounds with the use of automated CHNS analyzers. *Journal of analytical chemistry* **63**, 1094-1106 (2008).

41 Enders, A., Sohi, S., Lehmann, J. & Singh, B. Total elemental analysis of metals and nutrients in biochar. *Biochar: A Guide to Analytical Methods* **1** (2017).

42 Bakatula, E. N., Richard, D., Neculita, C. M. & Zagury, G. J. Determination of point of zero charge of natural organic materials. *Environmental Science and Pollution Research* **25**, 7823-7833, doi:10.1007/s11356-017-1115-7 (2018).

43 Gee, G. W. & Bauder, J. W. Particle-size analysis. *Methods of soil analysis: Part 1 Physical and mineralogical methods* **5**, 383-411 (1986).

44 Jackson, M. L. *Soil chemical analysis: advanced course*. (UW-Madison Libraries parallel press, 2005).

45 Dane, J. H. & Topp, C. G. *Methods of soil analysis, Part 4: Physical methods*. Vol. 20 (John Wiley & Sons, 2020).

46 Dahlquist, R. L. & Knoll, J. W. Inductively coupled plasma-atomic emission spectrometry: analysis of biological materials and soils for major, trace, and ultra-trace elements. *Applied Spectroscopy* **32**, 1-30 (1978).

47 Sparks, D. L., Page, A. L., Helmke, P. A. & Loeppert, R. H. *Methods of soil analysis, part 3: Chemical methods*. Vol. 14 (John Wiley & Sons, 2020).

48 Bettinelli, M., Beone, G. M., Spezia, S. & Baffi, C. Determination of heavy metals in soils and sediments by microwave-assisted digestion and inductively coupled plasma optical emission spectrometry analysis. *Analytica Chimica Acta* **424**, 289-296 (2000).

49 Piper, C. S. *Soil and plant analysis*. (Scientific Publishers, 2017).

50 Okebalama, C. B. & Marschner, B. Carbon and nutrient cycling responses to repeated application of biochar and NPK fertilizers depend on microenvironmental differences among hierarchical aggregate fractions. *Pedobiologia* **104**, 150962, doi:https://doi.org/10.1016/j.pedobi.2024.150962 (2024).

51 Hedley, M. J., Stewart, J. W. B. & Chauhan, B. Changes in inorganic and organic soil phosphorus fractions induced by cultivation practices and by laboratory incubations. *Soil Science Society of America Journal* **46**, 970-976 (1982).

52 Zhang, Y., Li, Y., Wang, S., Umbreen, S. & Zhou, C. Soil phosphorus fractionation and its association with soil phosphate-solubilizing bacteria in a chronosequence of vegetation restoration. *Ecological Engineering* **164**, 106208, doi:https://doi.org/10.1016/j.ecoleng.2021.106208 (2021).

53 Francis, C. A., Rutger, J. N. & Palmer, A. F. E. A rapid method for plant leaf area estimation in maize (Zea mays L.) 1. *Crop science* **9**, 537-539 (1969).

54 Iso, H. R. N. Soil quality-Pretreatment of samples for physico-chemical analysis. *HRN ISO* **11464** (2004).

55 Iso. Soil quality—Determination of dry matter and water content on a mass basis—Gravimetric method. *Beuth, Berlin* (1993).

56 Wong, J. W. C., Webber, J. B. W. & Ogbonnaya, U. O. Characteristics of biochar porosity by NMR and study of ammonium ion adsorption. *Journal of Analytical and Applied Pyrolysis* **143**, 104687, doi:https://doi.org/10.1016/j.jaap.2019.104687 (2019).

57 Mosa, A., El-Ghamry, A. & Tolba, M. Functionalized biochar derived from heavy metal rich feedstock: phosphate recovery and reusing the exhausted biochar as an enriched soil amendment. *Chemosphere* **198**, 351-363 (2018).

58 El-Banna, M. F. *et al.* Scavenging effect of oxidized biochar against the phytotoxicity of lead ions on hydroponically grown chicory: an anatomical and ultrastructural investigation. *Ecotoxicology and Environmental Safety* **170**, 363-374 (2019).

59 Zhang, S. & Wang, J. Removal of chlortetracycline from water by immobilized Bacillus subtilis on honeysuckle residue–derived biochar. *Water, Air, & Soil Pollution* **232**, 236, doi:10.1007/s11270-021-05193-1 (2021).

60 Zhang, K. *et al.* Biochar facilitated direct interspecies electron transfer in anaerobic digestion to alleviate antibiotics inhibition and enhance methanogenesis: A review. *International Journal of Environmental Research and Public Health* **20**, 2296 (2023).

61 Antor, N. H. *et al.* Chemically and biologically activated biochars slow down urea hydrolysis and improve nitrogen use efficiency. *Pedosphere* **33**, 659-669, doi:https://doi.org/10.1016/j.pedsph.2022.06.050 (2023).

62 Adapa, S. & Malani, A. Role of hydration energy and co-ions association on monovalent and divalent cations adsorption at mica-aqueous interface. *Scientific reports* **8**, 12198 (2018).

63 Anand, A., Gautam, S. & Ram, L. C. Feedstock and pyrolysis conditions affect suitability of biochar for various sustainable energy and environmental applications. *Journal of Analytical and Applied Pyrolysis* **170**, 105881, doi:https://doi.org/10.1016/j.jaap.2023.105881 (2023).

64 Phounglamcheik, A., Johnson, N., Kienzl, N., Strasser, C. & Umeki, K. Self-Heating of Biochar during Postproduction Storage by O2 Chemisorption at Low Temperatures. *Energies* **15**, 380 (2022).

65 Kanakalakshmi, A., Janaki, V., Shanthi, K., Kamala-Kannan, S. J. A. C., Nanomedicine, & Biotechnology. Biosynthesis of Cr (III) nanoparticles from electroplating wastewater using chromium-resistant Bacillus subtilis and its cytotoxicity and antibacterial activity. **45**, 1304-1309 (2017).

66 Wang, Y. *et al.* Remediation of Cd(II), Zn(II) and Pb(II) in contaminated soil by KMnO4 modified biochar: Stabilization efficiency and effects of freeze–thaw ageing. *Chemical Engineering Journal* **487**, 150619, doi:https://doi.org/10.1016/j.cej.2024.150619 (2024).

67 Alluqmani, S. M. *et al.* Preparation and characterisation of graphitic biochar materials derived from rose oil industry waste via different pyrolysis durations and ball milling for advanced composites. **11**, 035005 (2024).

68 Xiao, Y., Lyu, H., Tang, J., Wang, K. & Sun, H. Effects of ball milling on the photochemistry of biochar: Enrofloxacin degradation and possible mechanisms. *Chemical Engineering Journal* **384**, 123311, doi:https://doi.org/10.1016/j.cej.2019.123311 (2020).

69 Shaheen, S. M. *et al.* Manganese oxide-modified biochar: production, characterization and applications for the removal of pollutants from aqueous environments-a review. *Bioresource Technology* **346**, 126581 (2022).

70 Yuan, J.-H., Xu, R.-K. & Zhang, H. The forms of alkalis in the biochar produced from crop residues at different temperatures. *Bioresource Technology* **102**, 3488-3497, doi:https://doi.org/10.1016/j.biortech.2010.11.018 (2011).

71 Lyu, H. *et al.* Ball-milled biochar for alternative carbon electrode. **26**, 14693-14702 (2019).

72 Qu, X. *et al.* Chemical and structural properties of dissolved black carbon released from biochars. **96**, 759-767 (2016).

73 Eghtesadi, N. *et al.* Electroactivity of weak electricigen Bacillus subtilis biofilms in solution containing deep eutectic solvent components. *Bioelectrochemistry* **147**, 108207, doi:https://doi.org/10.1016/j.bioelechem.2022.108207 (2022).

74 Han, L. *et al.* Impact of biochar amendment on soil aggregation varied with incubation duration and biochar pyrolysis temperature. *Biochar* **3**, 339-347, doi:10.1007/s42773-021-00097-z (2021).

75 Ghorbani, M. & Amirahmadi, E. Insights into soil and biochar variations and their contribution to soil aggregate status – A meta-analysis. *Soil and Tillage Research* **244**, 106282, doi:https://doi.org/10.1016/j.still.2024.106282 (2024).

76 Cao, D. *et al.* Maize straw and its biochar affect phosphorus distribution in soil aggregates and are beneficial for improving phosphorus availability along the soil profile. *European Journal of Soil Science* **72**, 2165-2179 (2021).

77 Li, Q. *et al.* Effects of biochar on aggregate characteristics of upland red soil in subtropical China. *Environmental Earth Sciences* **76**, 372, doi:10.1007/s12665-017-6703-9 (2017).

78 Zhao, Z. *et al.* Release characteristics of phosphate from ball-milled biochar and its potential effects on plant growth. *Science of The Total Environment* **821**, 153256, doi:https://doi.org/10.1016/j.scitotenv.2022.153256 (2022).

79 Liu, Z., Ogunmokun, F. A. & Wallach, R. Does biochar affect soil wettability and flow pattern? *Geoderma* **417**, 115826, doi:https://doi.org/10.1016/j.geoderma.2022.115826 (2022).

80 Ng, C. W. W. *et al.* Effects of Bacillus subtilis and Pseudomonas fluorescens as the soil amendment. *Heliyon* **8**, e11674, doi:https://doi.org/10.1016/j.heliyon.2022.e11674 (2022).

81 Alhaj Hamoud, Y. *et al.* Increasing soil clay content increases soil phosphorus availability and improves the growth, physiology, and phosphorus uptake of rice under alternative wetting and mild drying irrigation. *Environmental Technology & Innovation* **35**, 103691, doi:https://doi.org/10.1016/j.eti.2024.103691 (2024).

82 Wang, Z. *et al.* Acid buffering capacity of four contrasting metal-contaminated calcareous soil types: Changes in soil metals and relevance to phytoextraction. *Chemosphere* **256**, 127045, doi:https://doi.org/10.1016/j.chemosphere.2020.127045 (2020).

83 Tian, J., Ge, F., Zhang, D., Deng, S. & Liu, X. Roles of phosphate solubilizing microorganisms from managing soil phosphorus deficiency to mediating biogeochemical P cycle. *Biology* **10**, 158 (2021).

84 Jin, X., Wang, S., Pang, Y. & Chang Wu, F. Phosphorus fractions and the effect of pH on the phosphorus release of the sediments from different trophic areas in Taihu Lake, China. *Environmental Pollution* **139**, 288-295, doi:https://doi.org/10.1016/j.envpol.2005.05.010 (2006).

85 Hinsinger, P., Plassard, C., Tang, C. & Jaillard, B. Origins of root-mediated pH changes in the rhizosphere and their responses to environmental constraints: a review. *Plant and soil* **248**, 43-59 (2003).

86 Liu, X.-H. & Zhang, X.-C. Effect of biochar on pH of alkaline soils in the loess plateau: results from incubation experiments. *International Journal of Agriculture & Biology* **14** (2012).

87 Novak, J. M. *et al.* Impact of biochar amendment on fertility of a southeastern coastal plain soil. *Soil science* **174**, 105-112 (2009).

88 Kumar, R. in *Biochar-Based Catalysts: Preparation, Characterization and Applications* 195-215 (Springer, 2024).

89 Su, J. *et al.* Mn-modified bamboo biochar improves soil quality and immobilizes heavy metals in contaminated soils. *Environmental Technology & Innovation* **34**, 103630, doi:https://doi.org/10.1016/j.eti.2024.103630 (2024).

90 Penn, C. J. & Camberato, J. J. A critical review on soil chemical processes that control how soil pH affects phosphorus availability to plants. *Agriculture* **9**, 120 (2019).

91 Chaganti, V. N., Crohn, D. M. & Šimůnek, J. J. A. W. M. Leaching and reclamation of a biochar and compost amended saline–sodic soil with moderate SAR reclaimed water. **158**, 255-265 (2015).

92 Sultan, H. *et al.* Biochar and nano biochar: Enhancing salt resilience in plants and soil while mitigating greenhouse gas emissions: A comprehensive review. *Journal of Environmental Management* **355**, 120448, doi:https://doi.org/10.1016/j.jenvman.2024.120448 (2024).

93 Lustosa Filho, J. F. *et al.* Aging of biochar-based fertilizers in soil: Effects on phosphorus pools and availability to Urochloa brizantha grass. *Science of The Total Environment* **709**, 136028, doi:https://doi.org/10.1016/j.scitotenv.2019.136028 (2020).

94 Hegab, O. A. & Abd El-Wahed, A. G. Origin of the glauconite from the Middle Eocene, Qarara Formation, Egypt. *Journal of African Earth Sciences* **123**, 21-28, doi:https://doi.org/10.1016/j.jafrearsci.2016.07.008 (2016).

95 Tang, Z. *et al.* New Insight into Phosphorus Release of Rhizosphere Soil in the Water Level Fluctuation Zone. *Sustainability* **15**, 6635 (2023).

96 Qetrani, S., Bouray, M. & Oukarroum, A. Phosphorus mobilization and acquisition in the alkaline-calcareous rhizosphere: A synthesis. *Rhizosphere* **30**, 100907, doi:https://doi.org/10.1016/j.rhisph.2024.100907 (2024).

97 Margalef, O. *et al.* Global patterns of phosphatase activity in natural soils. *Scientific reports* **7**, 1337 (2017).

98 Yuan, H. *et al.* Biochar's role as an electron shuttle for mediating soil N2O emissions. *Soil Biology and Biochemistry* **133**, 94-96, doi:https://doi.org/10.1016/j.soilbio.2019.03.002 (2019).

99 Lamar, R. T. Possible role for electron shuttling capacity in elicitation of PB activity of humic substances on plant growth enhancement. *The chemical biology of plant biostimulants*, 97-121 (2020).

100 Trazzi, P. A., Leahy, J. J., Hayes, M. H. B. & Kwapinski, W. Adsorption and desorption of phosphate on biochars. *Journal of environmental chemical engineering* **4**, 37-46 (2016).

101 Mosa, A., El-Ghamry, A. & Tolba, M. Biochar-supported natural zeolite composite for recovery and reuse of aqueous phosphate and humate: batch sorption–desorption and bioassay investigations. *Environmental Technology & Innovation* **19**, 100807 (2020).

102 Feng, C. *et al.* Bio-assembled MgO-coated tea waste biochar efficiently decontaminates phosphate from water and kitchen waste fermentation liquid. *Biochar* **5**, 22 (2023).

103 Lambers, H., Mougel, C., Jaillard, B. & Hinsinger, P. (Springer, 2009).

104 Khan, M. A. *et al.* Biochar optimizes wheat quality, yield, and nitrogen acquisition in low fertile calcareous soil treated with organic and mineral nitrogen fertilizers. **13**, 879788 (2022).
105 Khan, Z. *et al.* How biochar affects nitrogen assimilation and dynamics by interacting soil and plant enzymatic activities: quantitative assessment of 2 years potted study in a rapeseed-soil system. *Frontiers in Plant Science* **13**, 853449 (2022).

Declaration of interests

☒ The authors declare that they have no known competing financial interests or personal relationships that could have appeared to influence the work reported in this paper.

☒The authors declare the following financial interests/personal relationships which may be considered as potential competing interests:

Ahmed MoSa

Funding Declaration

This research was supported by the Mansoura University Research Fund (grant number MU-Agr-21-6). Partial funding was also provided by Academy of Scientific Research and Technology (Project ID: 14213). Finally, open access funding was provided by Science, Technology & Innovation Funding Authority (STDF) in cooperation with The Egyptian Knowledge Bank (EKB)

Figure Caption:

Fig. 1A: Physicochemical characterization of **functionalized** biochars. SEM-EDS spectra of pristine and **functionalized** biochar: a1(SEM micrograph of the pristine biochar), a2 (EDS spectra of the pristine biochar), a3 (SEM micrograph of chemically **functionalized** biochar), a4 (EDS spectra of chemically **functionalized** biochar), a5 (SEM micrograph of ball milled biochar), a6 (EDS spectra of ball milled biochar), a7 (SEM micrograph of biologically activated biochar), and a8 (EDS spectra of biologically activated biochar).

Fig. 1B: Physicochemical characterization of **functionalized** biochars: TGA curves of pristine and **functionalized** biochar (a), DSC thermograms of pristine and **functionalized** biochar (b), FTIR spectra of pristine and **functionalized** biochar (c), and XRD pattern of pristine and functionalized biochar (d). Original biochar (OB), chemically **functionalized** biochar (CHB), ball milled biochar (BMB) and biologically activated biochar (BIOB).

Fig. 2: SEM visualization imaging of soil-biochar interface after 30 days from incubation. Soil without biochar application (control), original biochar (OB), chemically **functionalized** biochar (CHB), ball milled biochar (BMB) and biologically activated biochar (BIOB).

Fig. 3: The distribution of soil phosphorus fractions as a percentage in different soil types after 30 days from incubation. Con (soil without biochar addition), P without biochar addition, OB (original biochar), CHB (chemically **functionalized** biochar), BMB (ball milled biochar), and BIOB (biologically activated biochar).

Fig. 4: Effect of **functionalized** biochar application on pH and EC values in different soil layers after maize harvesting. Con (soil without biochar addition), OB (original biochar), CHB (chemically **functionalized** biochar), BMB (ball milled biochar), and BIOB (biologically activated biochar).

Fig. 5: Effect of functionalized biochar application on available N (a), P (b) and K (c) retained in soil after maize harvesting in (mg kg^{-1}). Control (soil without biochar addition), OB (original biochar), CHB (chemically functionalized biochar), BMB (ball milled biochar), and BIOB (biologically activated biochar).

Fig. 6: The distribution of soil phosphorus fractions as a percentage in different soil layers after maize harvesting. Con (soil without biochar addition), OB (original

biochar), CHB (chemically **functionalized** biochar), BMB (ball milled biochar), and BIOB (biologically activated biochar).

Fig (1A):

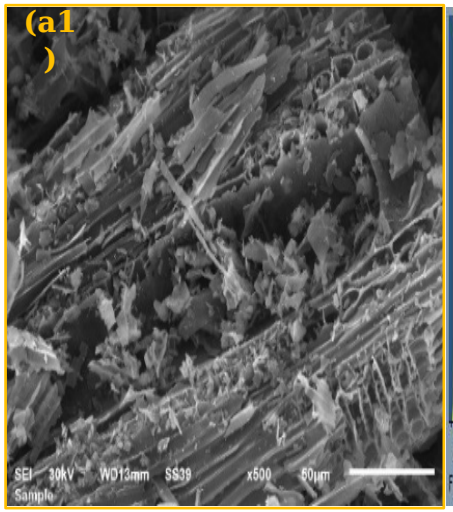

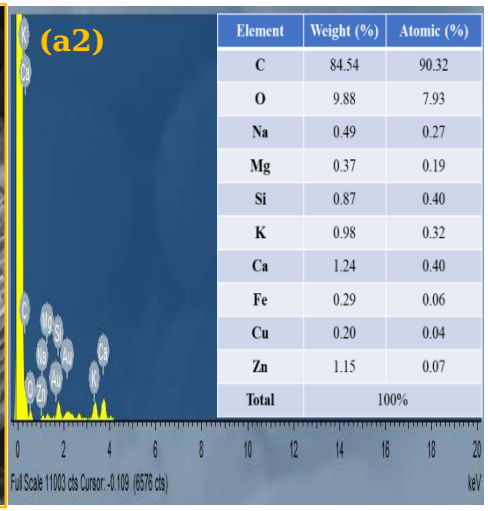

Element	Weight (%)	Atomic (%)
C	84.54	90.32
O	9.88	7.93
Na	0.49	0.27
Mg	0.37	0.19
Si	0.87	0.40
K	0.98	0.32
Ca	1.24	0.40
Fe	0.29	0.06
Cu	0.20	0.04
Zn	1.15	0.07
Total	100%	

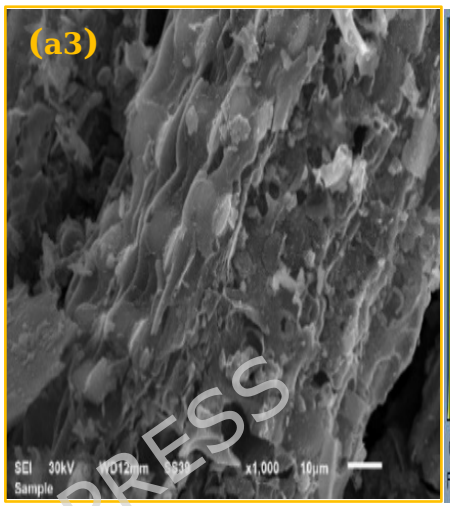

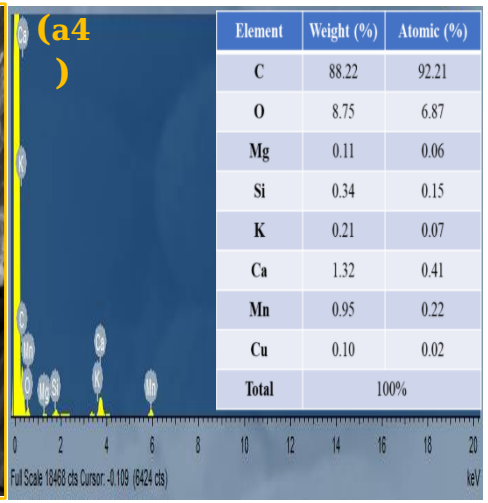

Element	Weight (%)	Atomic (%)
C	88.22	92.21
O	8.75	6.87
Mg	0.11	0.06
Si	0.34	0.15
K	0.21	0.07
Ca	1.32	0.41
Mn	0.95	0.22
Cu	0.10	0.02
Total	100%	

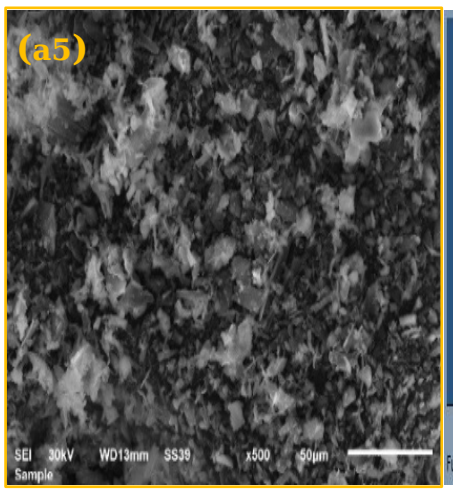

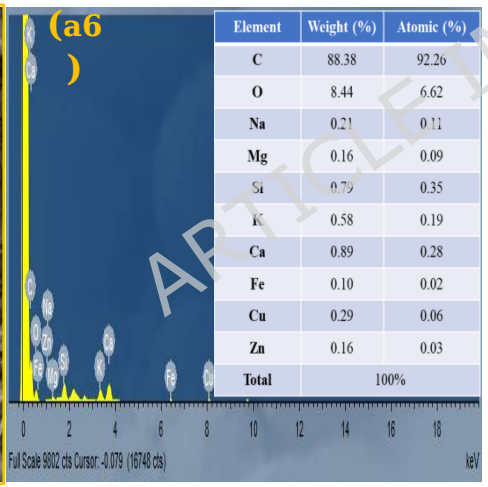

Element	Weight (%)	Atomic (%)
C	88.38	92.26
O	8.44	6.62
Na	0.21	0.11
Mg	0.16	0.09
Si	0.79	0.35
K	0.58	0.19
Ca	0.89	0.28
Fe	0.10	0.02
Cu	0.29	0.06
Zn	0.16	0.03
Total	100%	

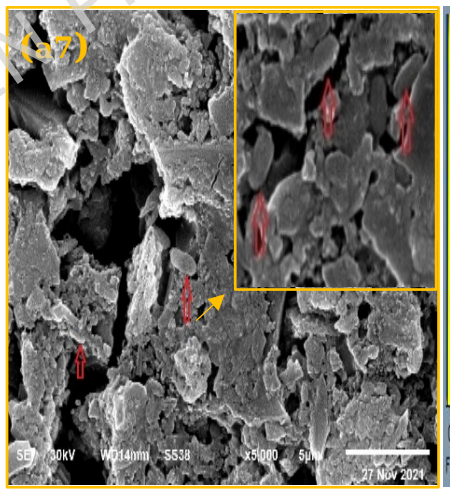

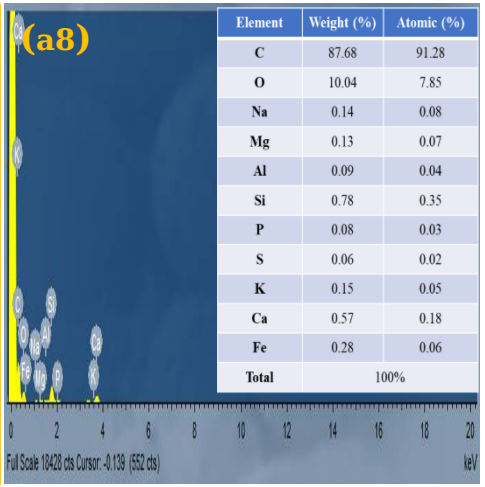

Element	Weight (%)	Atomic (%)
C	87.68	91.28
O	10.04	7.85
Na	0.14	0.08
Mg	0.13	0.07
Al	0.09	0.04
Si	0.78	0.35
P	0.08	0.03
S	0.06	0.02
K	0.15	0.05
Ca	0.57	0.18
Fe	0.28	0.06
Total	100%	

Fig

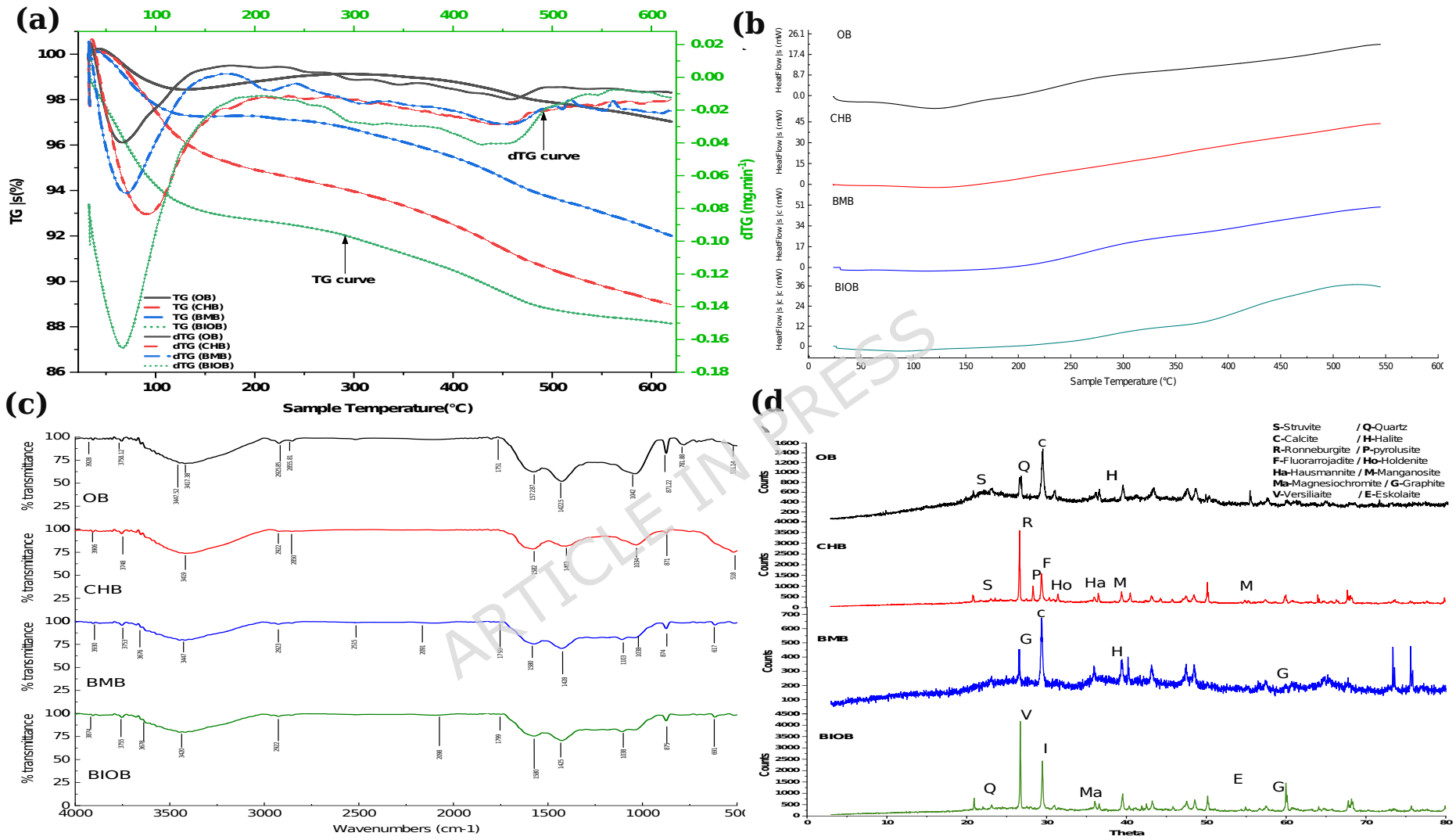

Fig. 2:

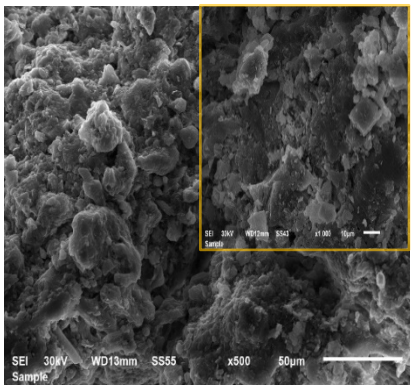

Pic (1): Soil (a)+ Control

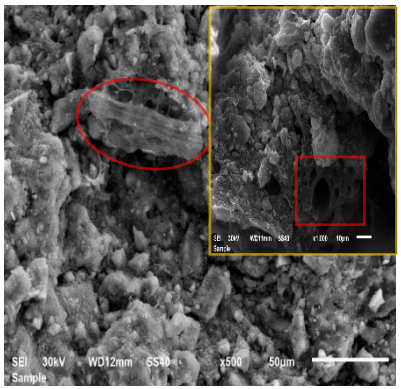

Pic (2): Soil (a)+ OB

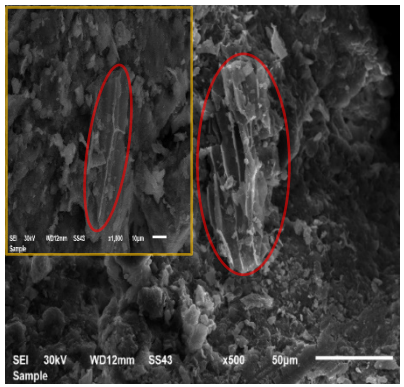

Pic (3): Soil (a)+ CHB

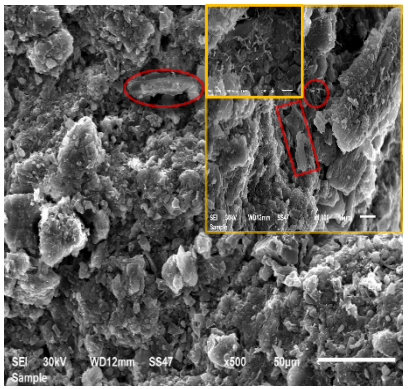

Pic (4): Soil (a)+ BMB

Pic (5): Soil (a)+ BIOB

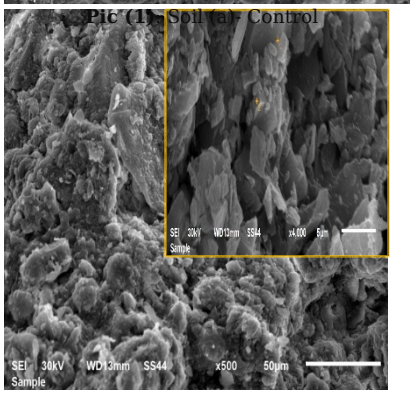

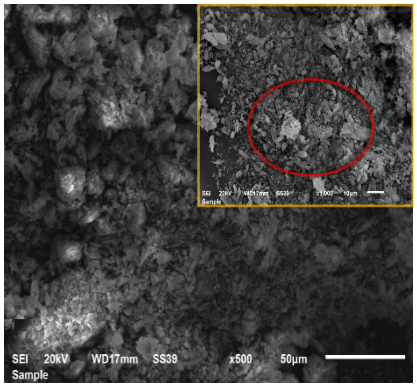

Pic (6): Soil (b)-Control

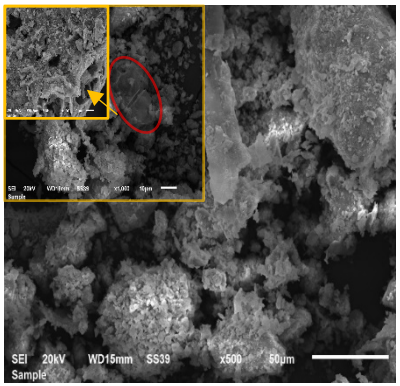

Pic (7): Soil (b)+ OB

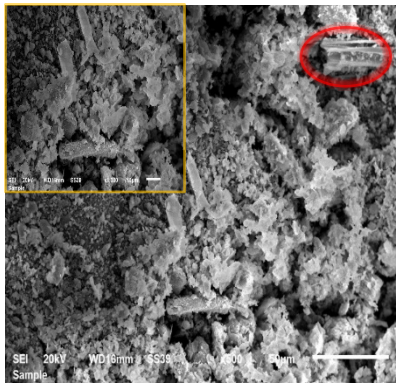

Pic (8): Soil (b)+ CHB

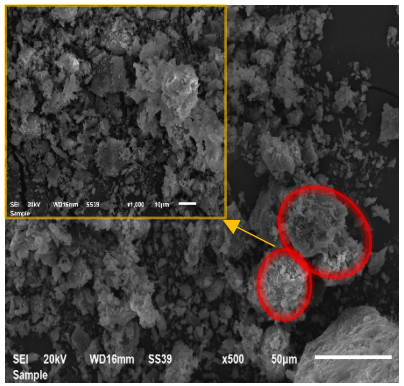

Pic (9): Soil (b)+ BMB

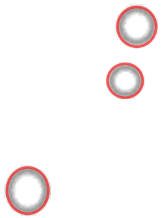

pic (10): Soil (b)+ BIOB

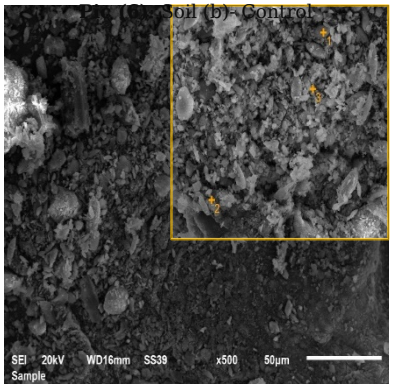

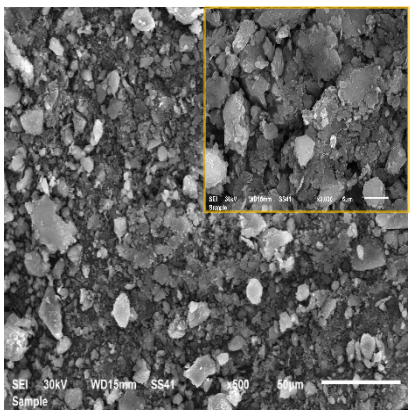

pic (11): Soil (c)-Control

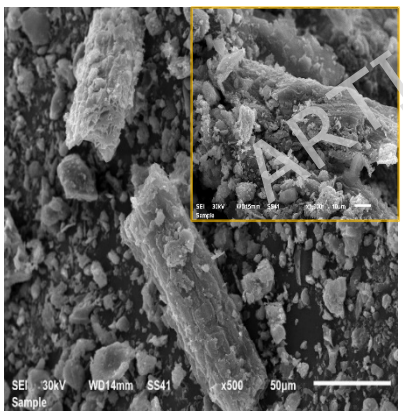

pic (12): Soil (c)+ OB

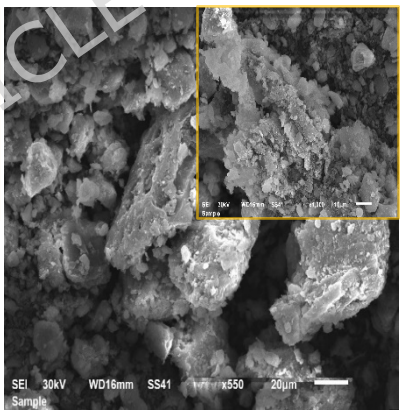

pic (13): Soil (c)+ CHB

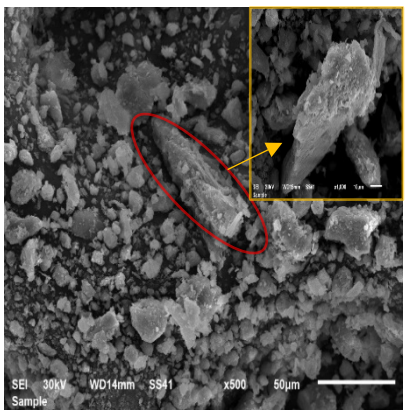

pic (14): Soil (c)+ BMB

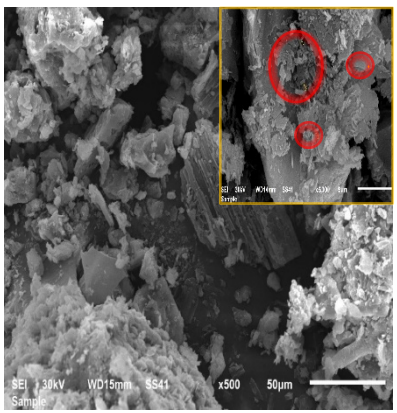

pic (15): Soil (c)+ BIOB

Fig. 3:

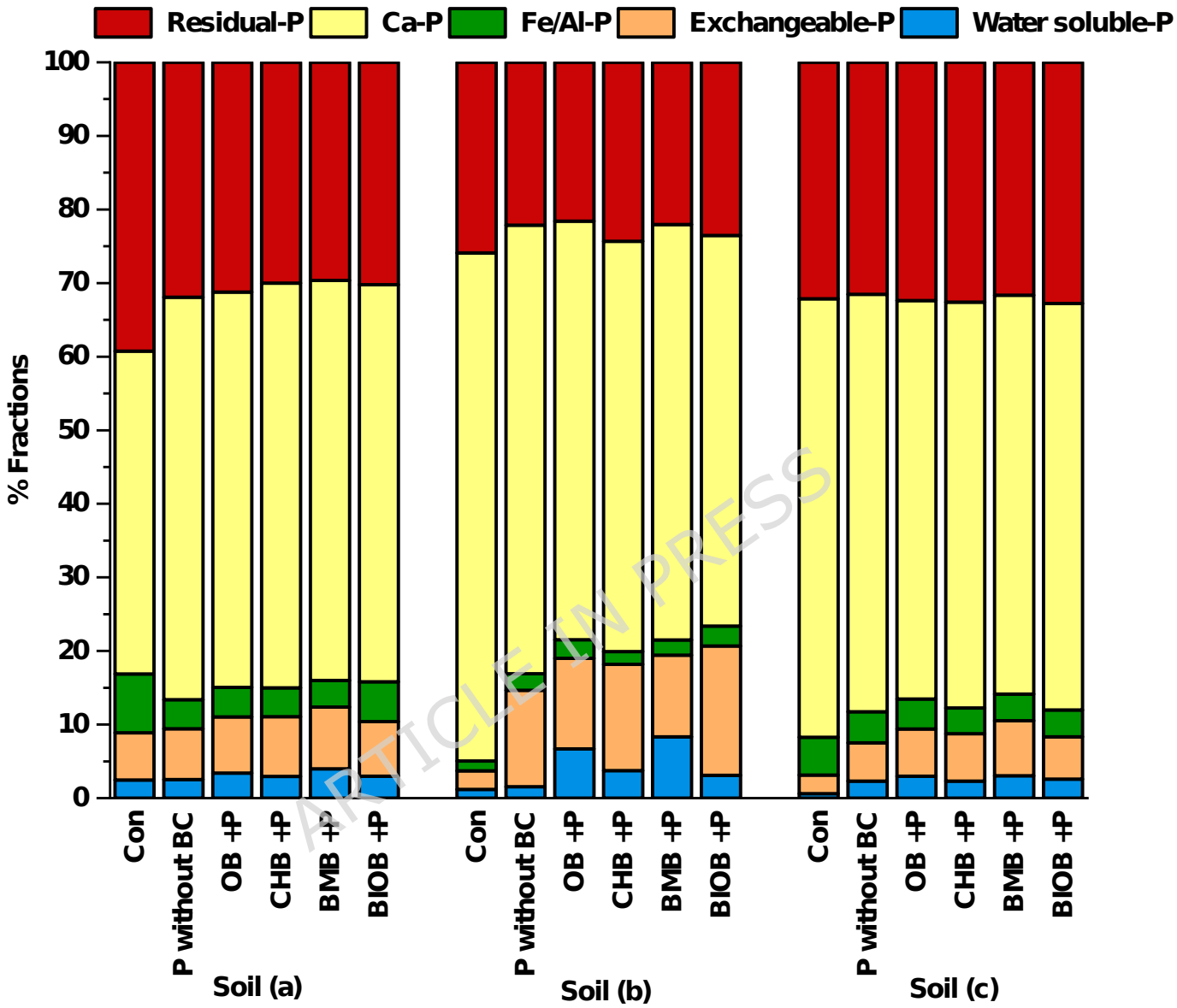

Fig. 4:

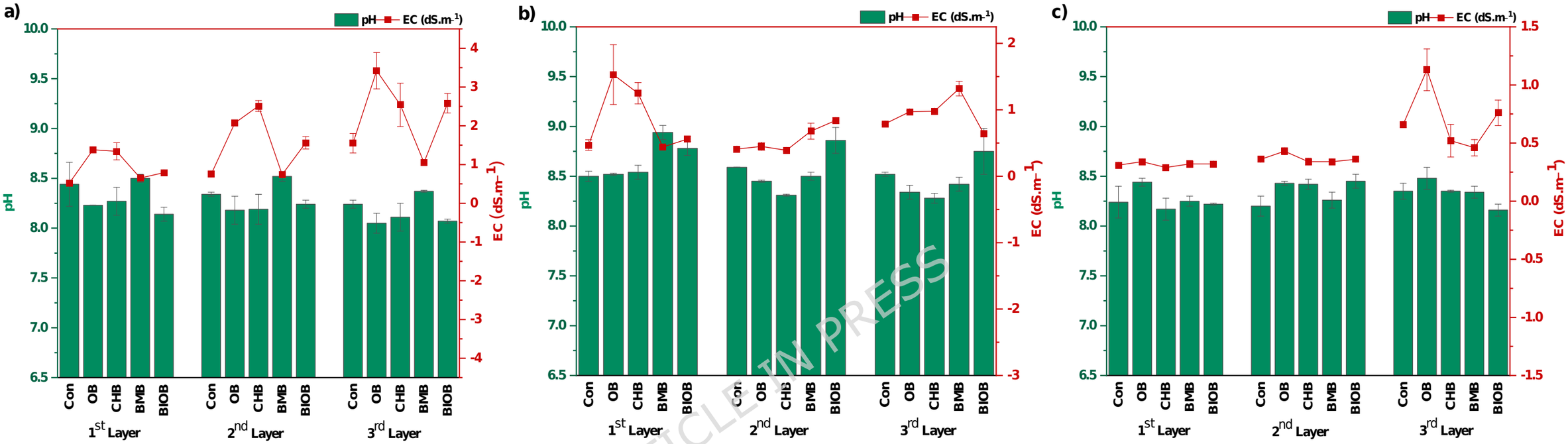

Fig .5:

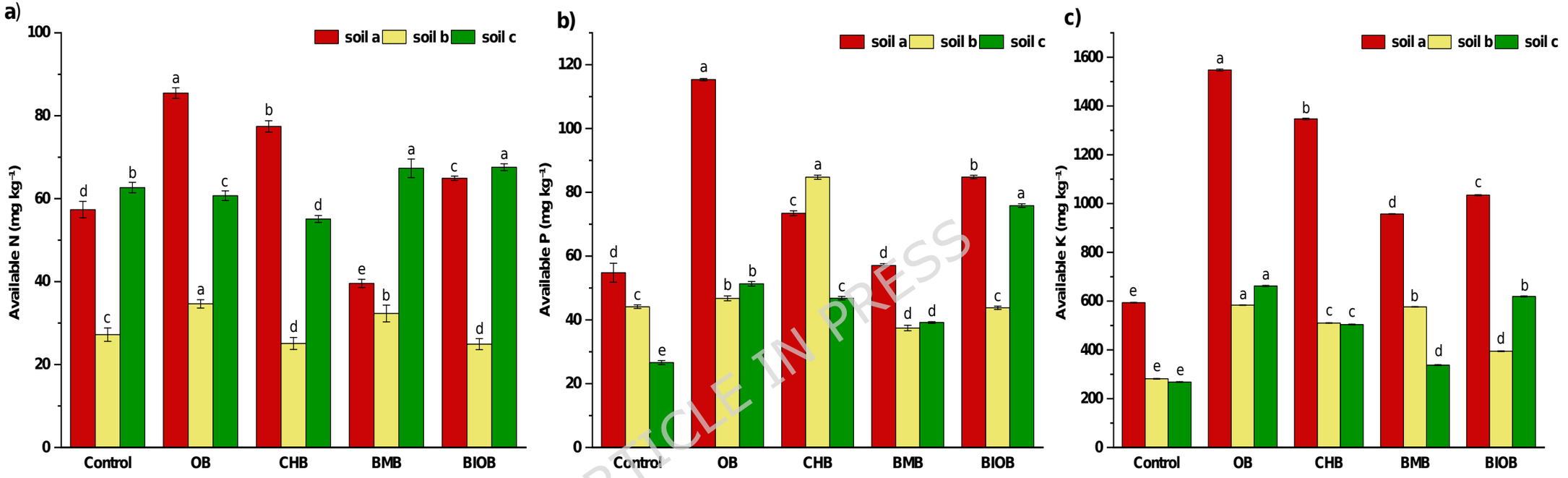

Fig. 6:

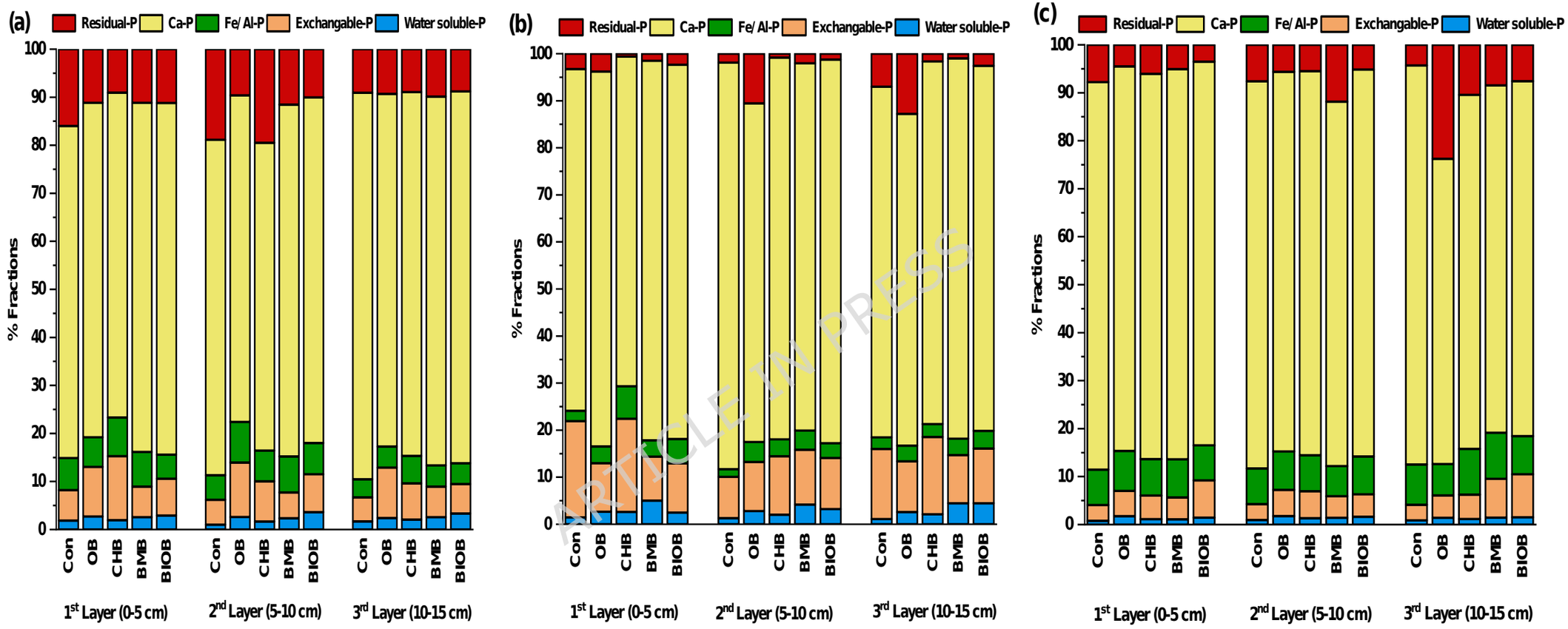

Table Captions:

Table. 1: Physical characteristics of pristine and **functionalized** biochar: Original biochar (OB), chemically functionalized biochar (CHB), ball milled biochar (BMB), and biologically **activated** biochar (BIOB).

Table. 2: Effect of **functionalized** biochars on soil aggregate fractions after 30 days from incubation.

Table. 3: Initial physical and chemical properties of soil types.

Table. 4: Effect of **functionalized biochars** on vegetative growth parameters and nutrients concentration in maize seedlings.

Table. 1:

Biochar types	Surface area (m^2 g^{-1})	Total pore volume (cm^3 g^{-1})	Pore diameter (nm)	Zeta Potential (ζ) (mV)
OB	40.78 ±0.27	0.068 ±0.001	1.92 ±0.008	-17.1 ±7.37
BMB	22.44 ±1.00	0.049 ±0.01	1.92 ±0.004	-15.36 ±4.39
CHB	29.21 ±0.30	0.061 ±0.01	1.91 ±0.001	-15.30 ±0.52
BIOB	34.69 ±0.42	0.069 ±0.004	1.92 ±0.001	-25.03 ±0.70

Values are means of three replicates ± standard deviation. Biochar types are original biochar (OB), chemically **functionalized** biochar (CHB), ball milled biochar (BMB), and biologically **activated** biochar (BIOB)

Table. 2:

Sample	Treatment	2 – 0.25 mm				0.25-0.05mm			<0.05 mm	**MWD**
		>1mm	**1 – 0.5 mm**	**0.5-0.25 mm**	**Sum**	**0.25-0.1 mm**	**1-0.05 mm**	**Sum**		
Soil (b)	Control	47.18± 1.6 b	27.85 ±0.54 b	14.40 ±0.86 b	89.44 ±1.51 a	7.83 ±1.21 c	2.71 ±0.38 b	10.53 ±1.60 c	0.96 ±0.18 b	51.07 ±0.62 ab
	OB	35.82± 0.88 c	29.65 ±1.17 a	18.48 ±0.27 a	83.97 ±0.48 bc	10.72 ±0.96 a	3.27 ±0.85 a	13.99 ±0.92 a	1.53 ±0.19 a	49.41 ±1.08 c
	CHB	45.65± 1.07 b	25.65 ±0.49 c	14.13 ±1.62 b	85.45 ±1.28 b	8.89 ±0.96 b	2.90 ±0.38 ab	11.79 ±0.84 b	1.44 ±0.26 a	50.56 ±0.48 b
	BMB	35.11± 2.91 c	28.95 ±1.07 a	18.21 ±1.07 a	82.28 ±2.55 c	6.22 ±0.61 d	2.65 ±0.34 b	8.86 ±0.83 d	1.02 ±0.13 b	51.48 ±0.40 a
	BIOB	56.31± 3.61 a	22.82 ±0.53 d	11.00 ±0.77 c	90.13 ±2.77 a	6.45 ±0.76 d	2.84 ±0.41 ab	9.29 ±1.17 d	1.39 ±0.19 a	50.62 ±0.65 b
Soil (b)	Control	3.78± 0.93 bc	11.56 ±0.38 bc	26.73 ±0.48 c	42.08 ±0.51 d	36.29 ±0.97 c	14.79 ±0.09 d	51.09 ±0.93 b	4.39 ±0.48 a	28.71 ±0.48 c
	OB	3.03± 0.11 d	10.99 ±0.87 c	29.16 ±0.31 a	43.19 ±0.61 c	39.47 ±0.55 a	15.75 ±0.29 b	55.22 ±0.47 a	1.03 ±0.04 c	28.72 ±0.46 c
	CHB	3.43± 0.71 cd	12.14 ±2.33 b	28.06 ±0.28 b	43.63 ±2.29 c	38.34 ±0.49 b	16.71 ±0.44 a	55.05 ±0.81 a	0.94 ±0.04 c	28.89 ±0.13 c
	BMB	3.93± 0.04 b	13.37 ±0.92 a	28.00 ±0.35 b	45.31 ±0.81 b	36.14 ±0.48 c	15.27 ±0.13 c	51.42 ±0.43 b	1.35 ±0.19 b	30.42 ±1.10 b
	BIOB	6.27± 0.27 a	14.36 ±0.08 a	26.76 ±0.41 c	47.40 ±0.73 a	36.41 ±0.51 c	14.68 ±0.55 d	51.09 ±0.04 b	0.68 ±0.11 d	31.15 ±0.11 a
Soil (c)	Control	47.06 ±1.45 a	25.93 ±1.84 d	13.53 ±1.05 b	86.53 ±2.91 a	6.76 ±0.26 c	3.37 ±0.07 c	10.14 ±0.34 c	4.63 ±0.92 a	51.54 ±0.58 a
	OB	36.46 ±0.92 d	31.23 ±0.29 a	17.34 ±1.27 a	85.04 ±2.06 a	8.03 ±0.88 b	3.92 ±0.71 b	11.95 ±1.37 b	0.94 ±0.13 b	50.23 ±0.29 b
	CHB	34.97 ±1.75 e	29.92 ±0.06 b	14.92 ±1.96 b	79.83 ±0.24 c	7.02 ±1.24 c	3.12 ±0.65 c	10.14 ±1.89 c	0.92 ±0.08 b	51.58 ±0.44 a
	BMB	42.61 ±1.17 b	27.86 ±1.35 c	15.29 ±0.61 b	85.77 ±0.67 a	9.23 ±0.69 a	4.69 ±0.38 a	13.93 ±1.07 a	1.24 ±0.75 b	49.31 ±0.24 c
	BIOB	38.23 ±0.65 c	29.01 ±0.55 b	14.76 ±3.81 b	82.01 ±3.30 b	8.70 ±0.07 ab	4.57 ±0.06 a	13.27 ±0.01 a	0.91 ±0.18 b	50.31 ±0.43 b

Values are mean of three replicates ± standard deviation. Mean values followed by the same letter are not significantly different at p=0.05 according to LSD test. Soil without biochar application (control), original biochar (OB), chemically functionalized biochar (CHB), ball milled biochar (BMB), and biologically activated biochar (BIOB).

Table. 3:

Parameter	Unit	Soil (a)	Soil (b)	Soil (c)
Texture		**Clay Loam**	**Sandy Clay Loam**	**Silty Loam**
Sand		31.10	62.82	42.00
Silt	**%**	37.40	9.02	50.00
Clay		31.50	28.15	8.00
pH	**------**	7.85	8.13	8.09
EC	**dS m⁻¹**	2.57	1.608	1.32
$CaCO_3$	**%**	3.20	12.47	2.90
Total C	**%**	1.45	0.33	0.44
Available-N	**mg kg⁻¹**	110.95	21.42	57.84
Available-P	**mg kg⁻¹**	39.39	2.90	5.60
Available-K	**mg kg⁻¹**	565.44	407.59	169.49
Zn	**mg kg⁻¹**	284.95	314.76	243.35
Mn	**mg kg⁻¹**	796.26	211.30	853.90
Cd	**mg kg⁻¹**	4.93	2.14	5.05
Pb	**mg kg⁻¹**	13.45	29.77	10.05
Ni	**mg kg⁻¹**	34.66	19.37	34.82
As	**mg kg⁻¹**	**N D**	**N D**	5.36

N. D means not detected

Table. 4:

Sample	Treatment	Fresh Weight (g)	Dry Weight (g)	Leaf area (cm^2)	Longest Leaf (cm)	Plant height (cm)	% Total Nitrogen	% Total phosphorus	% Total Potassium
Soil (a)	Control	22.57±2.54 b	2.35 ±0.28 a	48.64 ±1.04 d	23.25 ±1.17 d	44.87 ±2.25 a	2.36 ± 0.24 a	0.16 ±0.01 b	5.34 ±0.93 c
	OB	16.74 ±2.4 c	2.38 ±0.34 a	53.56 ±0.80 c	25.75 ±1.50 c	36.92 ±3.5 c	2.31 ± 0.47 a	0.18 ±0.01 b	5.29 ± 0.53 c
	CHB	26.94 ±1.91 a	2.43 ±0.03 a	65.34 ±1.74 b	30.33 ±0.67 b	44.71 ±2.92 a	1.77 ± 0.09 b	0.24 ±0.02 a	6.25 ± 0.17 b
	BMB	27.62 ±1.88 a	2.68 ±0.46 a	67.02 ±1.78 a	30.92 ±0.83 b	41.08 ±1.5 b	1.85 ± 0.25 b	0.25 ±0.03 a	7.51 ± 0.06 a
	BIOB	26.11 ±1.46 a	2.54 ±0.58 a	43.70 ±0.10 e	33.75 ±1.50 a	44.08 ±1.7 a	2.48 ± 0.41 a	0.16 ±0.05 a	7.46 ± 0.44 a
Soil (b)	Control	5.03 ±1.70 c	0.16 ±0.09 e	19.56 ±2.07 c	13.91 ±1.49 c	17.38 ±0.64 e	1.36 ± 0.08 bc	0.11 ±0.06 d	5.42 ± 0.87 b
	OB	11.39 ±0.88 ab	0.72 ±0.02 b	23.38 ±1.67 b	23.92 ±1.83 a	34.92 ±0.83 a	1.39 ±0.21 bc	0.21 ±0.05 b	7.09 ± 0.24 a
	CHB	10.92 ±0.84 b	0.42 ±0.01 c	22.08 ±2.16 b	24.03 ±0.73 a	32.22 ±1.25 b	3.29 ± 0.45 a	0.17 ±0.001 c	5.62 ± 0.62 b
	BMB	11.85 ±0.79 a	0.27 ±0.03 d	15.03 ±1.67 d	22.86 ±0.73 ab	26.70 ±0.93 d	1.41 ± 0.03 b	0.18 ±0.07 a	6.67 ± 0.21 a
	BIOB	10.66 ±0.39 b	1.48 ±0.06 a	26.43 ±2.39 a	21.83 ±1.33 b	31.16 ±3.48 c	1.18 ± 0.13 c	0.20 ±0.03 bc	4.53 ± 0.71 c
Soil (c)	Control	11.54 ±0.57 d	0.58 ±0.17 d	28.39 ±0.96 c	25.02 ±0.30 c	31.62 ±1.10 d	1.85 ± 0.28 b	0.14 ±0.003 a	5.36 ± 0.27 d
	OB	19.52 ±0.62 b	1.78 ±0.24 bc	47.19 ±4.61 a	27.94 ±3.94 b	37.00 ±0.66 c	2.01 ±0.02 b	0.16 ± 0.005 a	7.52 ± 0.50 a
	CHB	16.73 ±0.91 c	1.47 ±0.14 c	43.88 ±1.54 b	28.89 ±4.03 b	36.99 ±2.65 c	1.23 ±0.04 c	0.16 ± 0.001 a	5.91 ± 0.01 c
	BMB	21.56 ±0.71 a	2.57 ±0.71 a	43.74 ±1.66 b	27.81 ±0.95 b	43.73 ±1.37 a	2.42 ±0.28 a	0.15 ± 0.004 a	6.32 ± 0.22 b
	BIOB	21.45 ±0.82 a	1.91 ±0.08 b	41.85 ±2.72 b	32.25 ±1.61 a	42.16 ±1.33 b	1.38 ± 0.11 c	0.14 ± 0.005 a	6.10 ± 0.17 bc

Values are mean of three replicates ± standard deviation. Mean values followed by the same letter are not significantly different at p=0.05 according to LSD test. Soil without biochar application (control), original biochar (OB), chemically **functionalized** biochar (CHB), ball-milled biochar (BMB), and biologically activated biochar (BIOB)